Turbulent Flows

Stephen B. Pope

Cambridge University Press, 2000

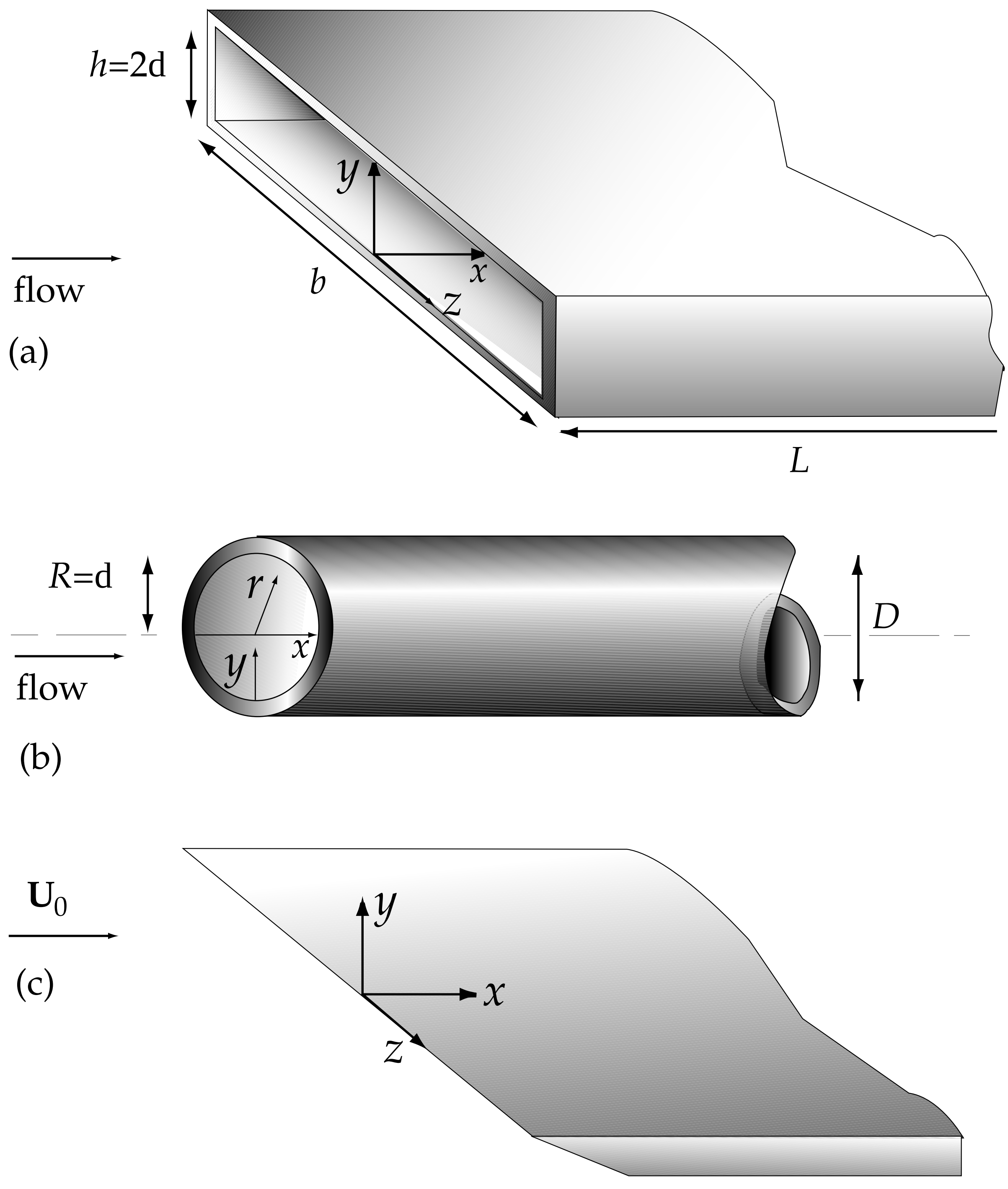

Figure 7.1: Sketch of (a) channel flow (b) pipe flow and (c) flat-plate boundary layer.

Turbulent Flows

Stephen B. Pope
Cambridge University Press, 2000

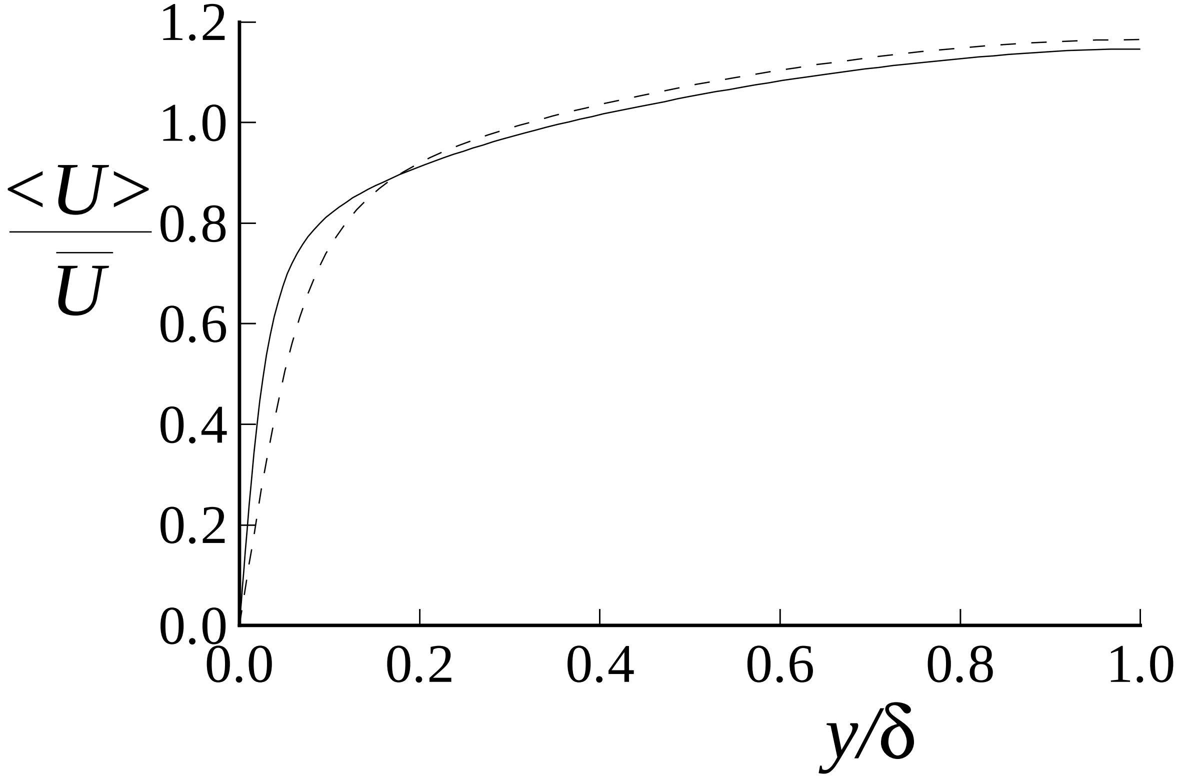

Figure 7.2: Mean velocity profiles in fully-developed turbulent channel flow from the DNS of Kim *et al.* (1987): dashed line, Re $= 5,600$; solid line, Re $= 13,750$

Turbulent Flows

Stephen B. Pope
Cambridge University Press, 2000

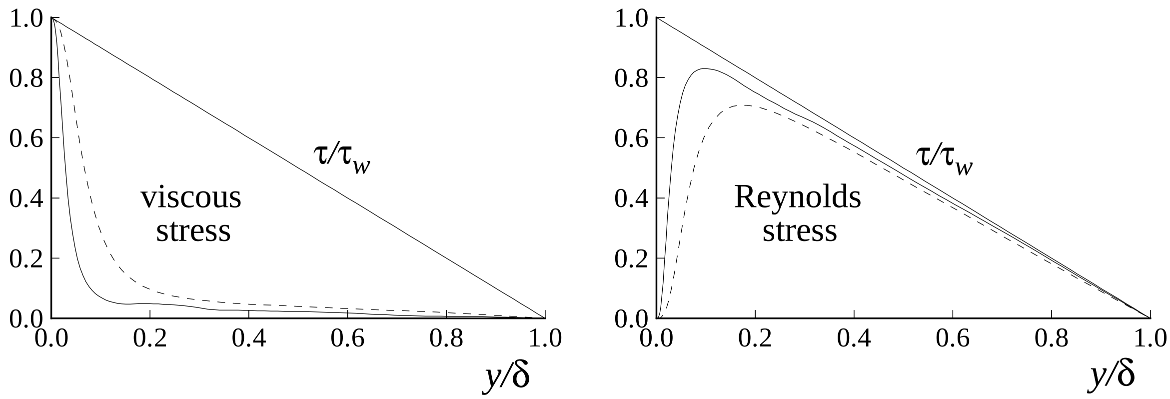

Figure 7.3: Profiles of the viscous shear stress, and the Reynolds shear stress in turbulent channel flow: DNS data of Kim *et al.* (1987): dashed line, $\mathrm{Re} = 5,600$; solid line, $\mathrm{Re} = 13,750$.

Turbulent Flows

Stephen B. Pope
Cambridge University Press, 2000

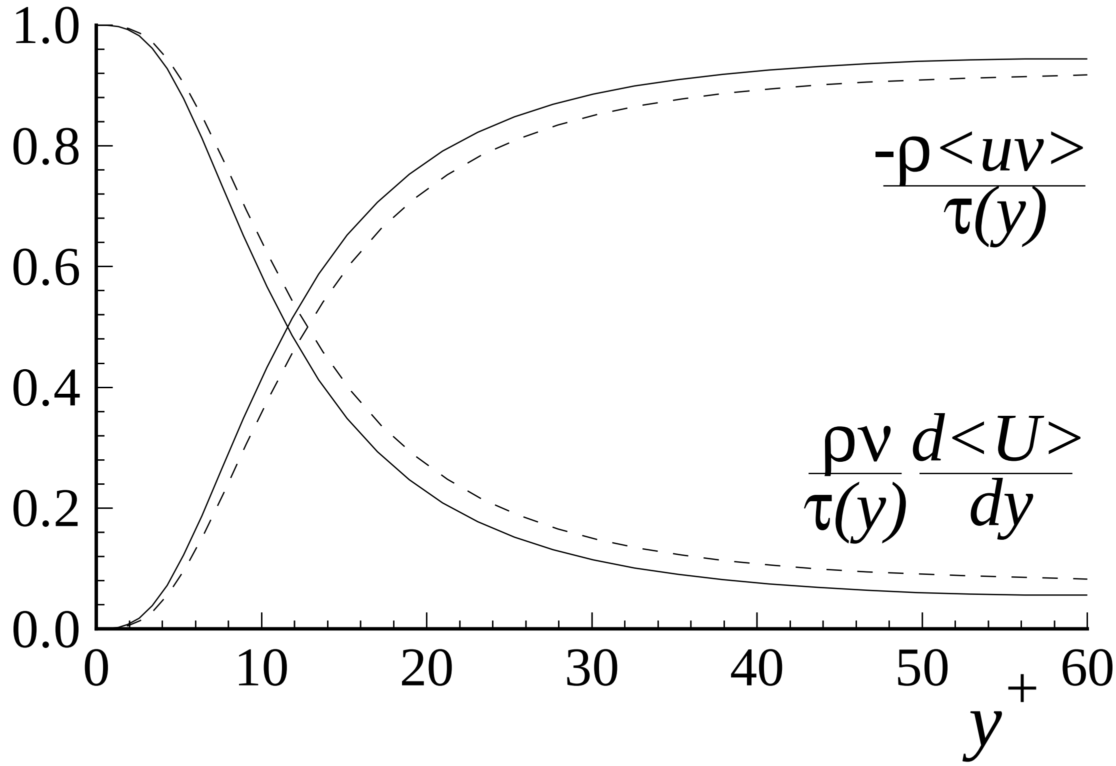

Figure 7.4: Profiles of the fractional contributions of the viscous and Reynolds stresses to the total stress. DNS data of Kim *et al.* (1987): dashed lines, Re $= 5,600$; solid lines, Re $= 13,750$.

Turbulent Flows

Stephen B. Pope
Cambridge University Press, 2000

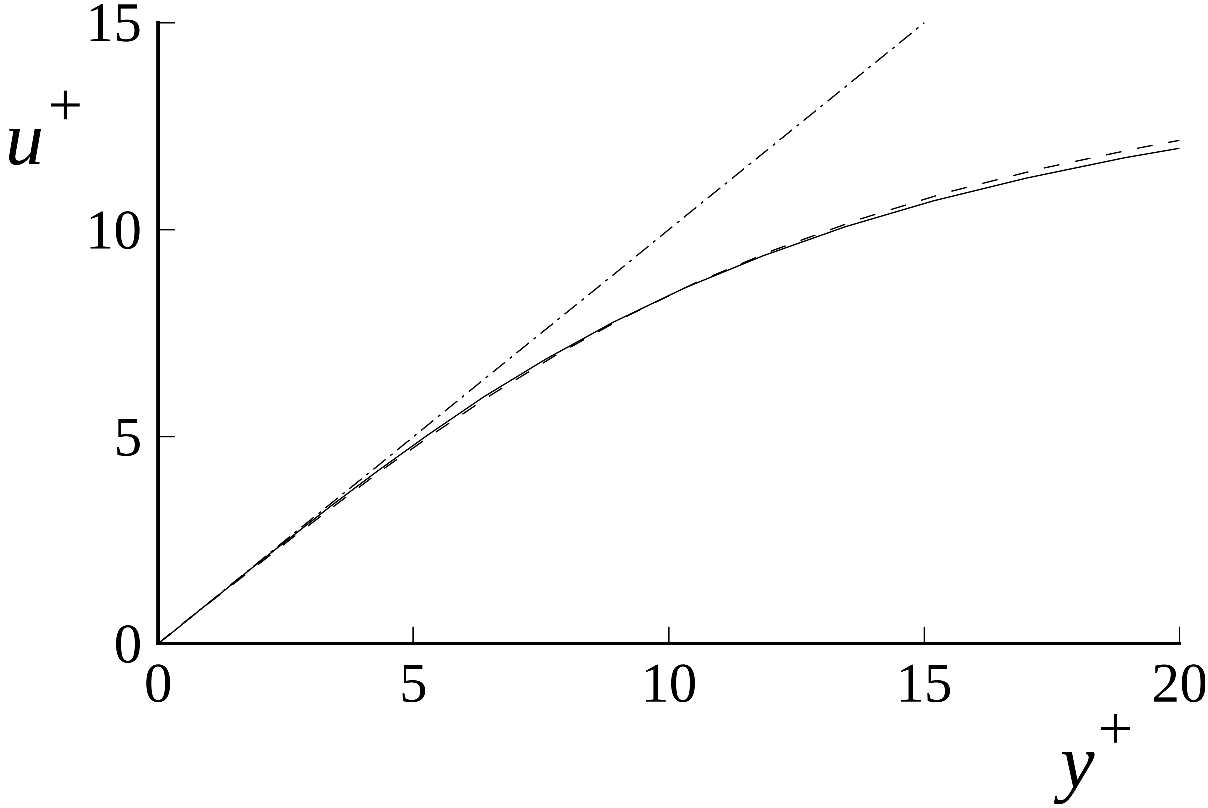

Figure 7.5: Near-wall profiles of mean velocity from the DNS data of Kim *et al.*: dashed line, Re $= 5,600$; solid line, Re $= 13,750$; dot-dashed line, $u^+ = y^+$.

Turbulent Flows

Stephen B. Pope
Cambridge University Press, 2000

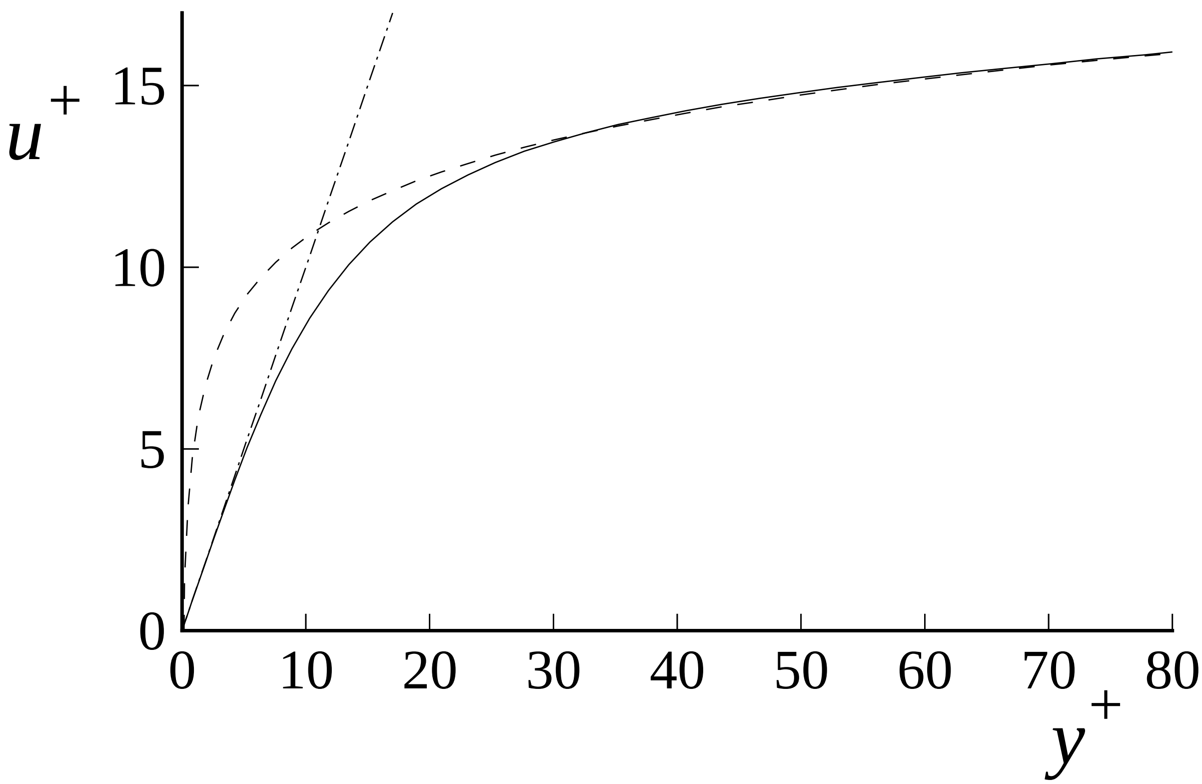

Figure 7.6: Near-wall profiles of mean velocity: solid line, DNS data of Kim *et al.*: Re $= 13,750$; dot-dashed line, $u^+ = y^+$; dashed line, the log law, Eqs. (7.43)–(7.44).

Turbulent Flows

Stephen B. Pope
Cambridge University Press, 2000

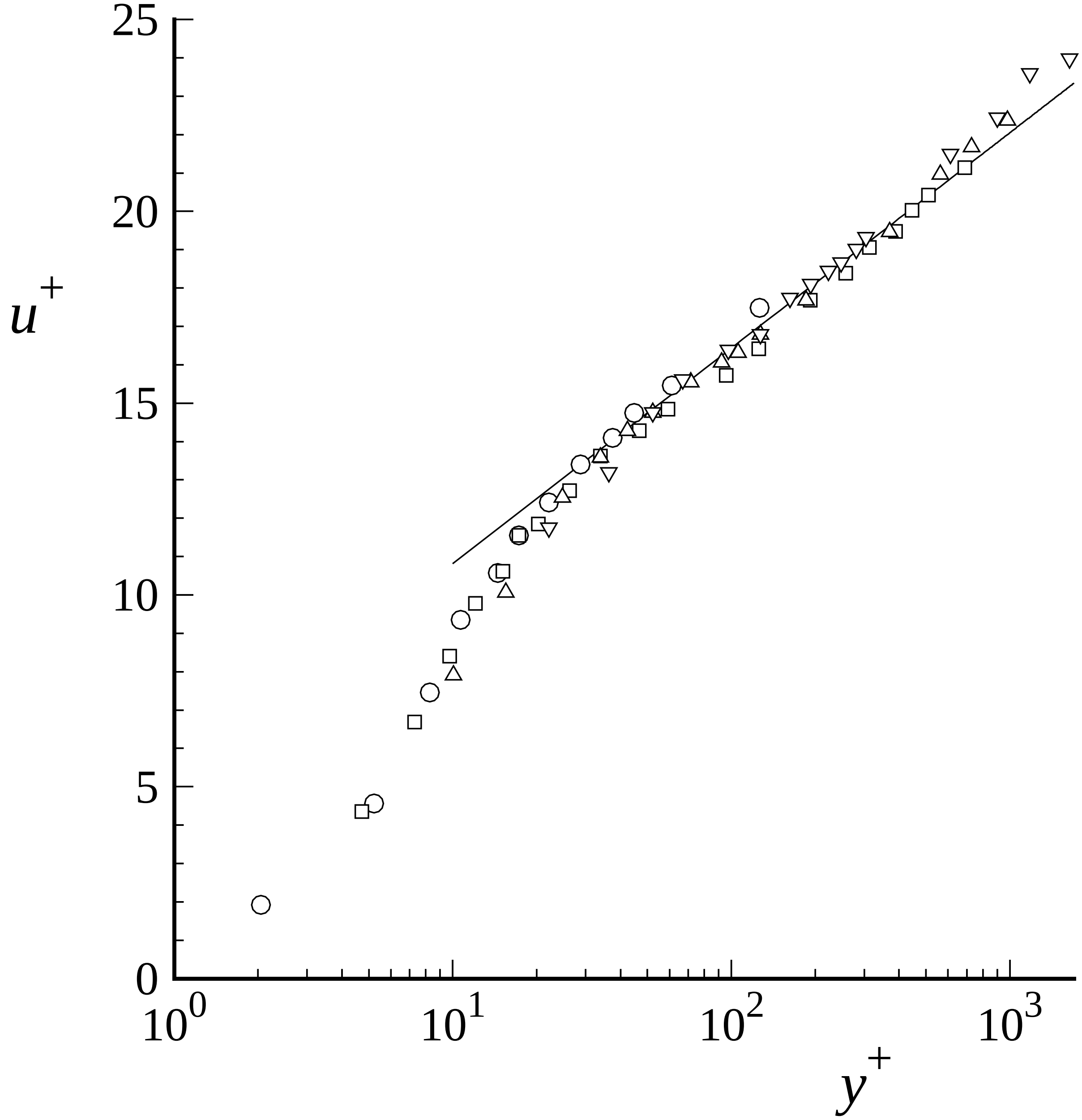

Figure 7.7: Mean velocity profiles in fully-developed turbulent channel flow measured by Wei and Willmarth (1989): $\circ$, $\mathrm{Re}_0 = 2,970$; $\square$, $\mathrm{Re}_0 = 14,914$; Δ, $\mathrm{Re}_0 = 22,776$; ∇, $\mathrm{Re}_0 = 39,582$; line, the log law, Eqs. (7.43)–(7.44).

Turbulent Flows

Stephen B. Pope
Cambridge University Press, 2000

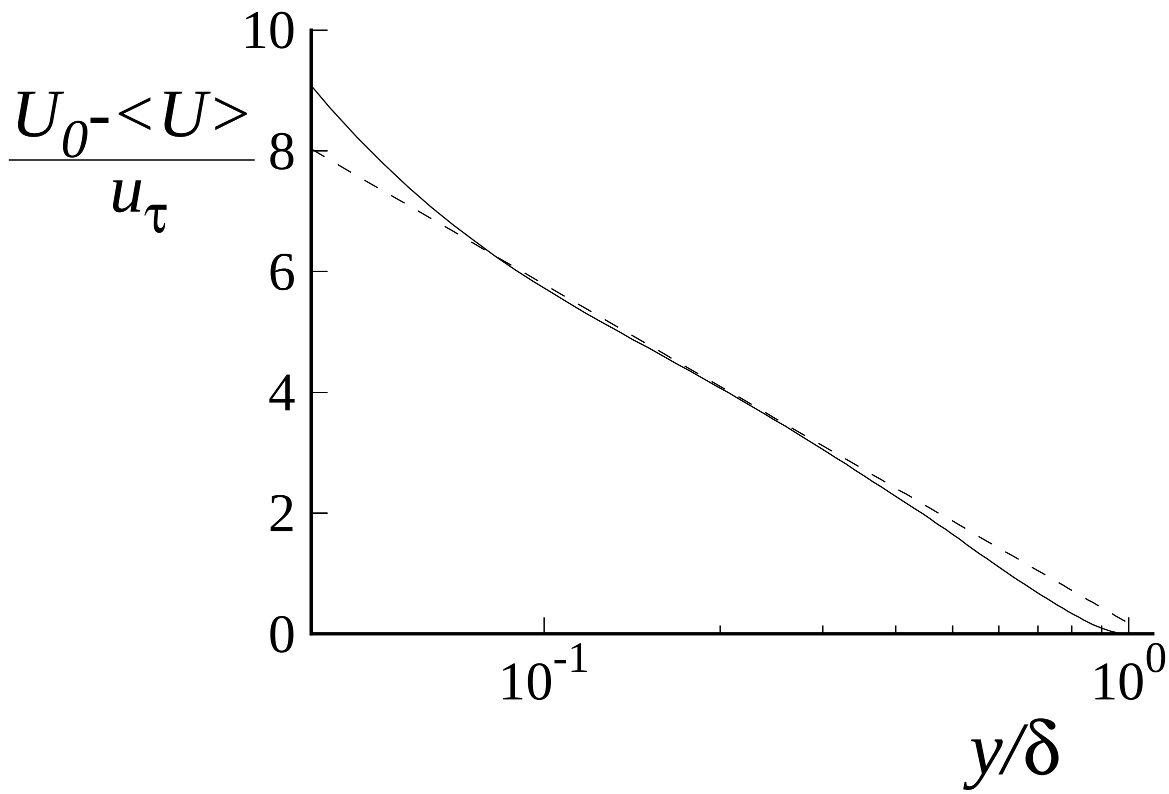

Figure 7.9: Mean velocity defect in turbulent channel flow. Solid line, DNS of Kim *et al.* (1987), Re $= 13,750$; dashed line, log law, Eqs. (7.43)–(7.44).

Turbulent Flows

Stephen B. Pope
Cambridge University Press, 2000

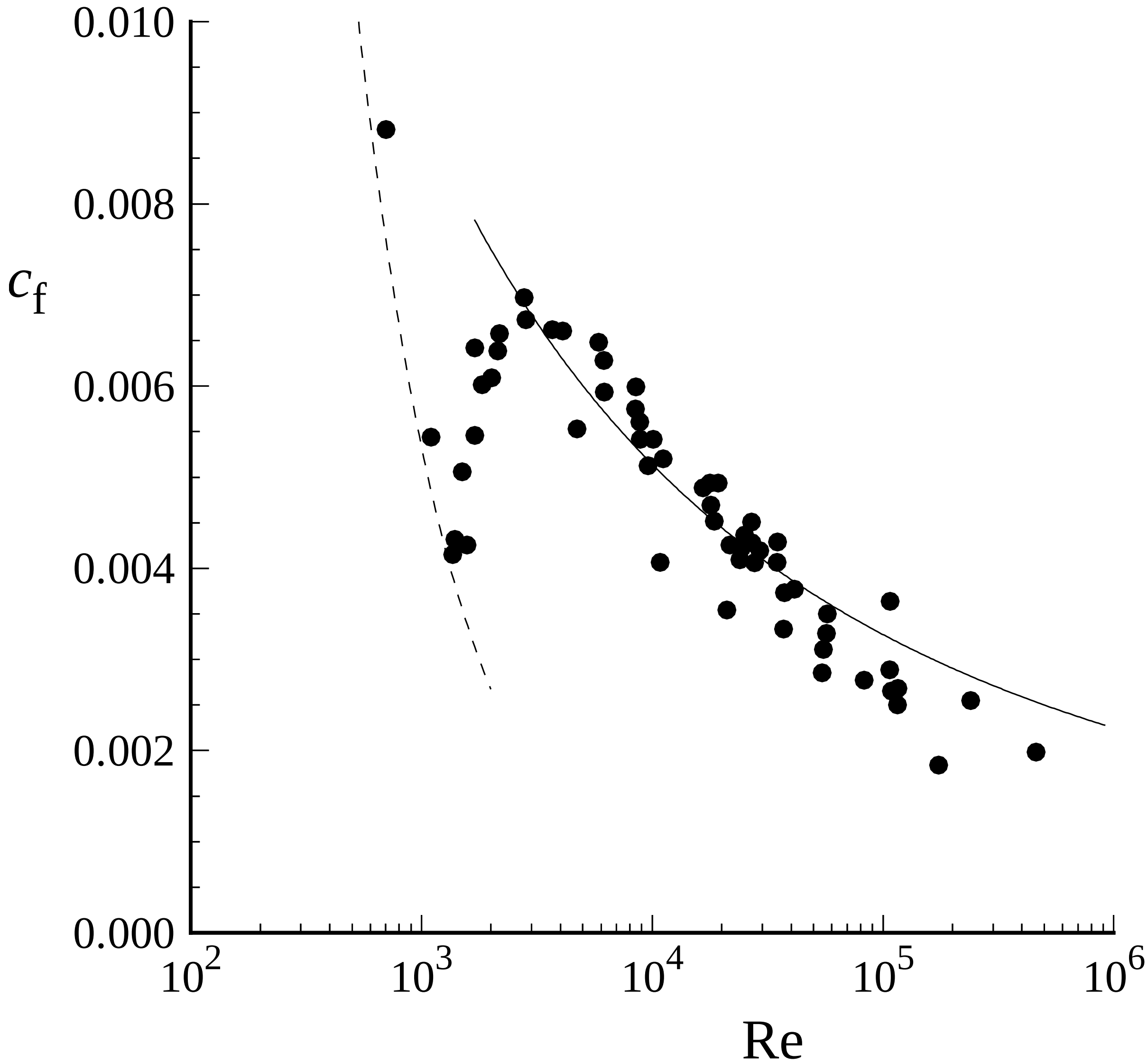

Figure 7.10: Skin friction coefficient $c_f \equiv \tau_w/(\frac{1}{2}\rho U_0^2)$ against Reynolds number ($\mathrm{Re} = 2\bar{U}\delta/\nu$) for channel flow: symbols, experimental data compiled by Dean (1978); solid line, from Eq. (7.55); dashed line, laminar friction law $c_f = 16/(3Re)$.

Turbulent Flows

Stephen B. Pope
Cambridge University Press, 2000

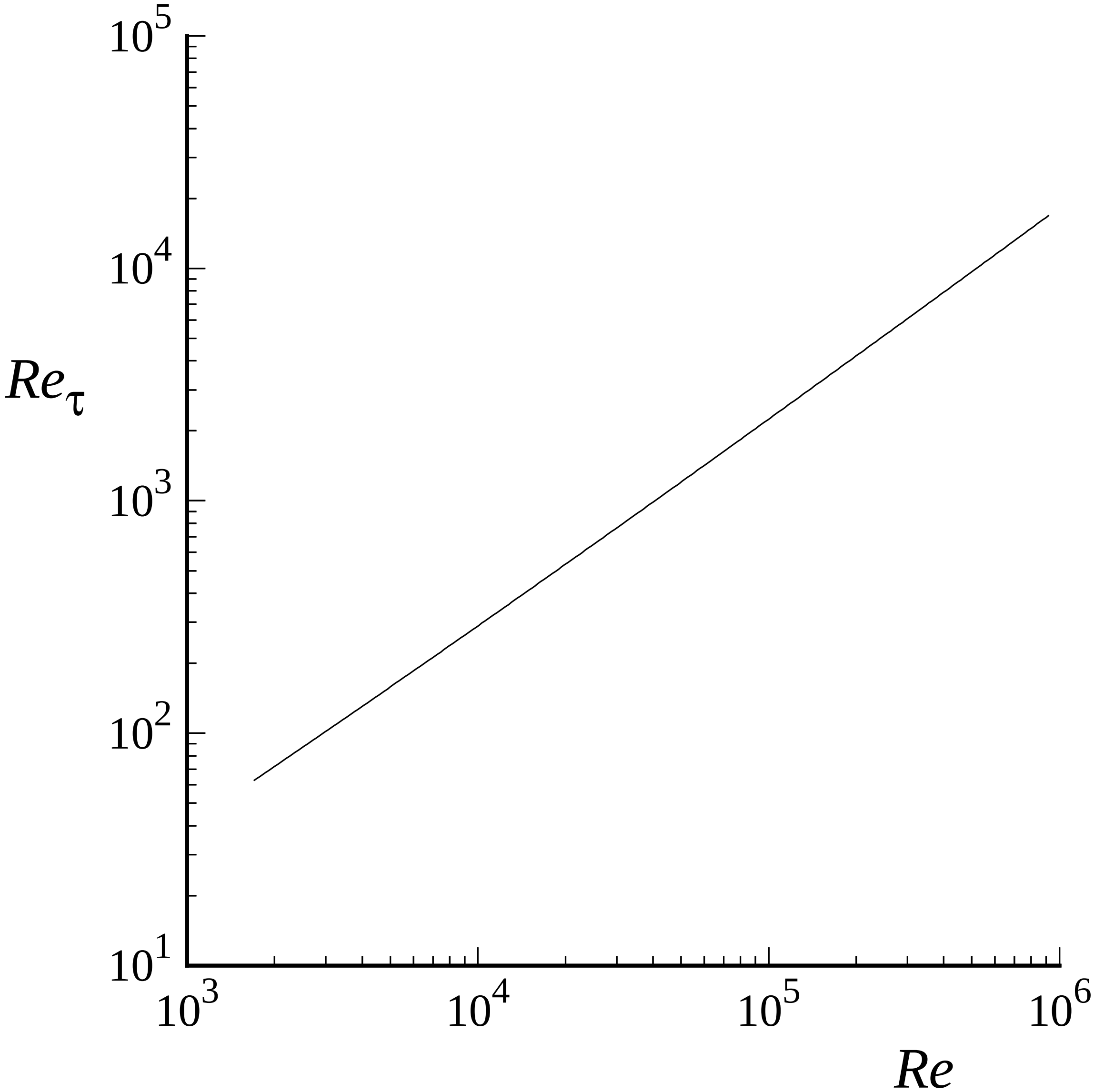

Figure 7.11: Outer-to-inner lengthscale ratio $\delta/\delta_\nu = \mathrm{Re}_\tau$ for turbulent channel flow as a function of Reynolds number (obtained from Eq. 7.55).

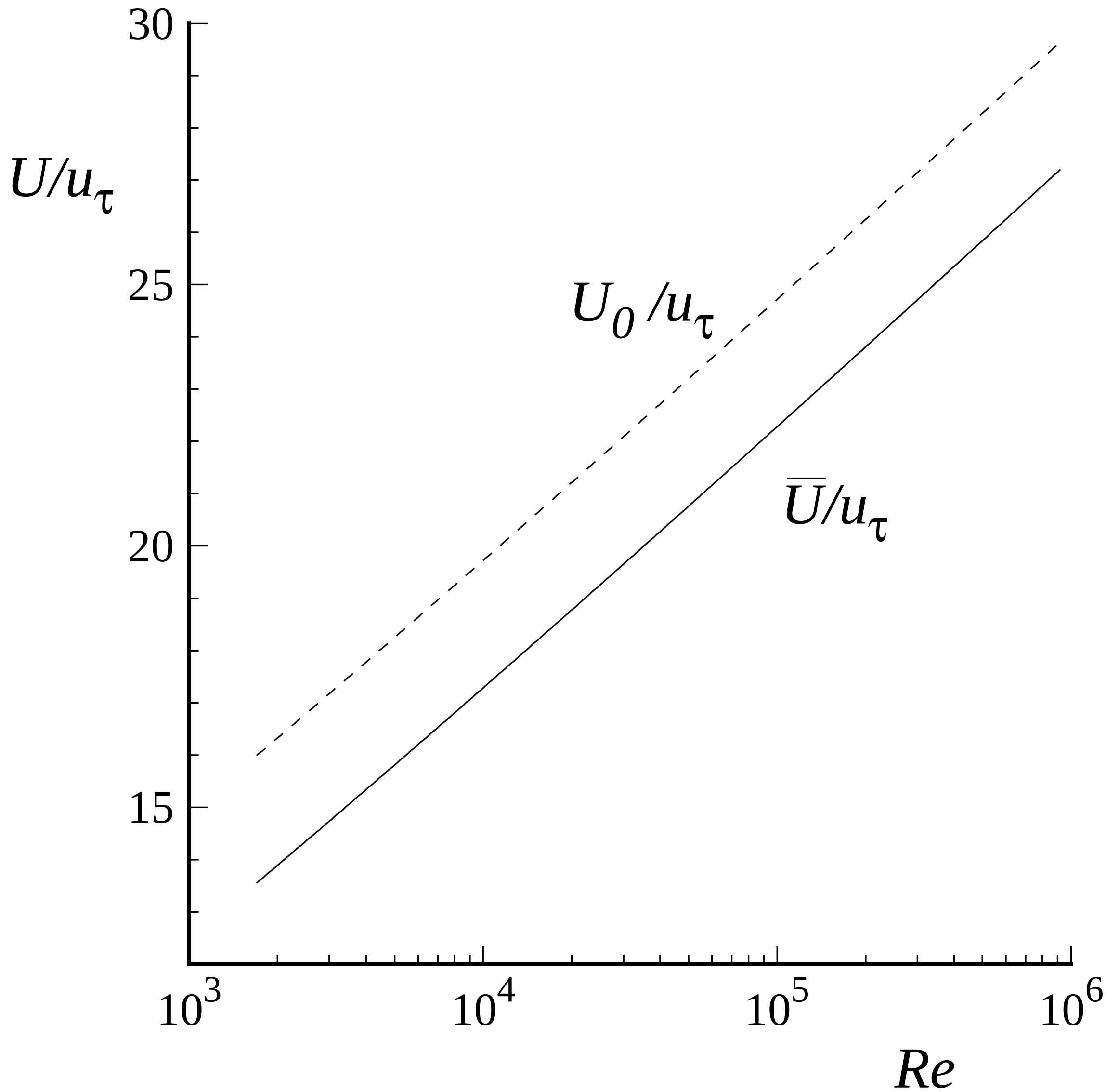

Figure 7.12: Outer-to-inner velocity scale ratios for turbulent channel flow as functions of Reynolds number (obtained from Eq. 7.55): solid line, $\bar{U}/u_\tau$; dashed line U_0/u_τ.

Turbulent Flows

Stephen B. Pope
Cambridge University Press, 2000

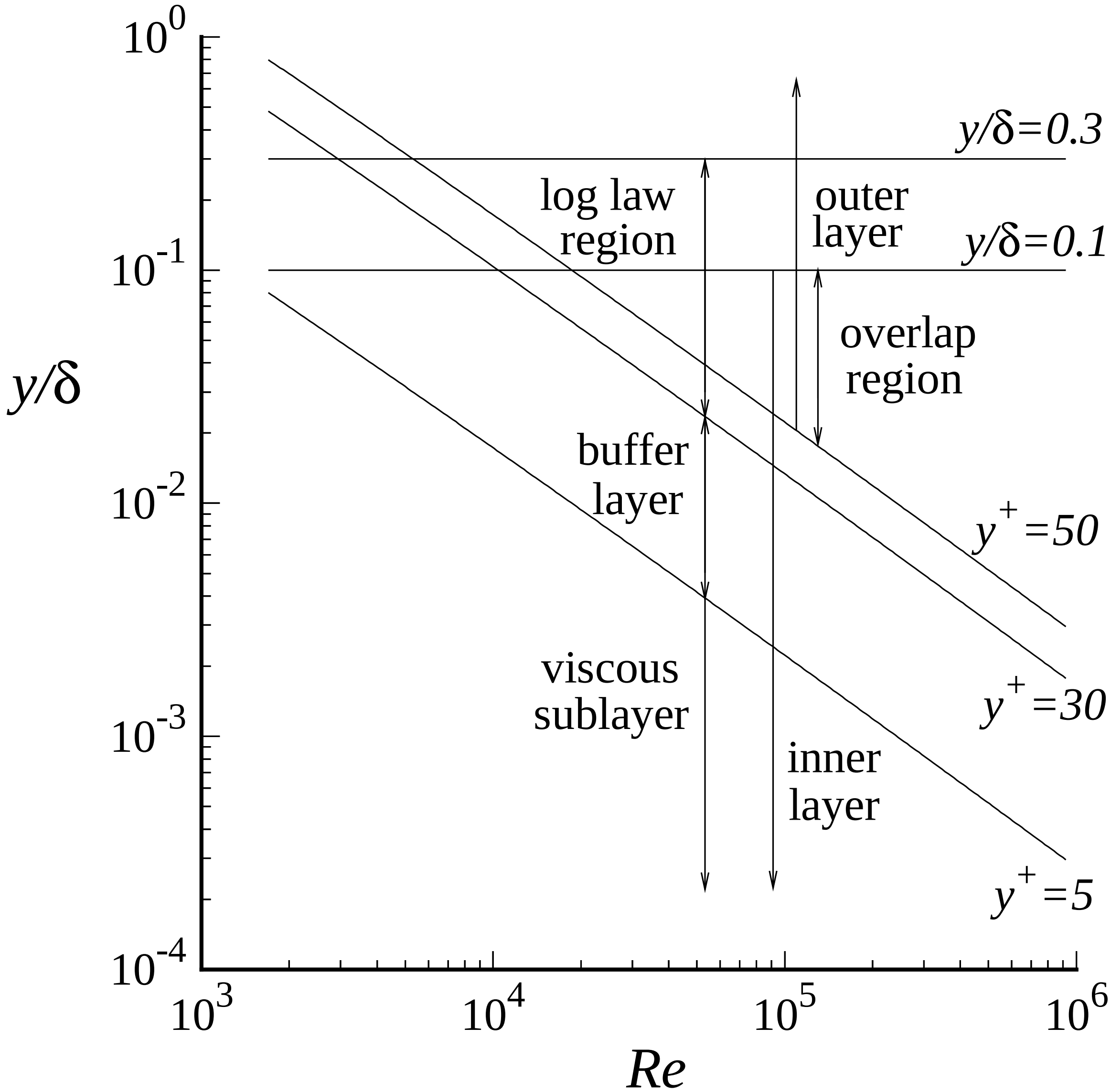

Figure 7.13: Regions and layers in turbulent channel flow as functions of Reynolds number.

Turbulent Flows

Stephen B. Pope
Cambridge University Press, 2000

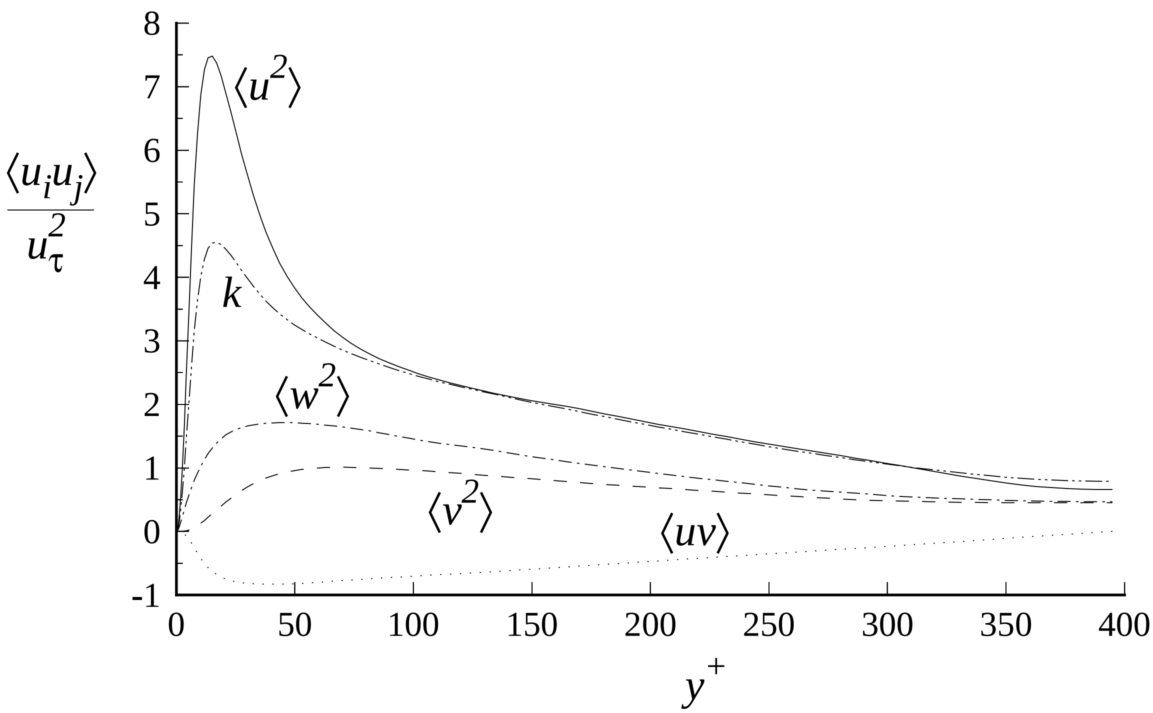

Figure 7.14: Reynolds stresses and kinetic energy normalized by friction velocity against y^+ from DNS of channel flow at $\mathrm{Re} = 13,750$ (Kim *et al.* 1987).

Turbulent Flows

Stephen B. Pope
Cambridge University Press, 2000

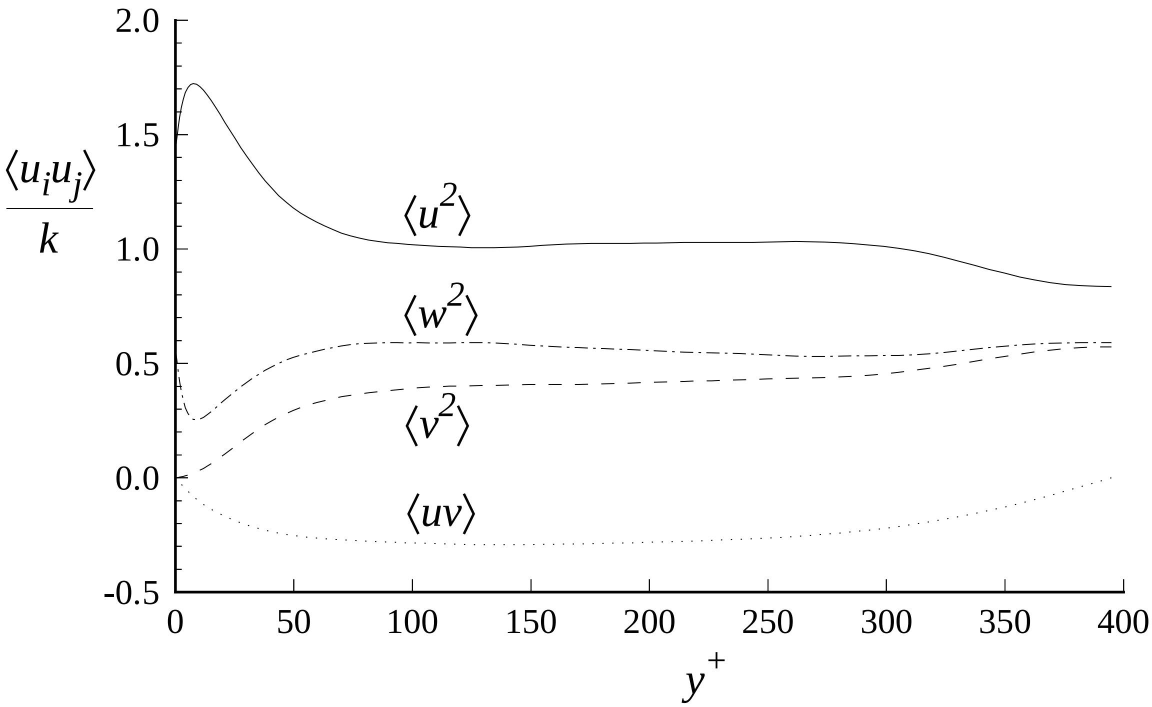

Figure 7.15: Profiles of Reynolds stresses normalized by turbulent kinetic energy from DNS of channel flow at $\mathrm{Re} = 13,750$ (Kim *et al.* 1987).

Turbulent Flows

Stephen B. Pope
Cambridge University Press, 2000

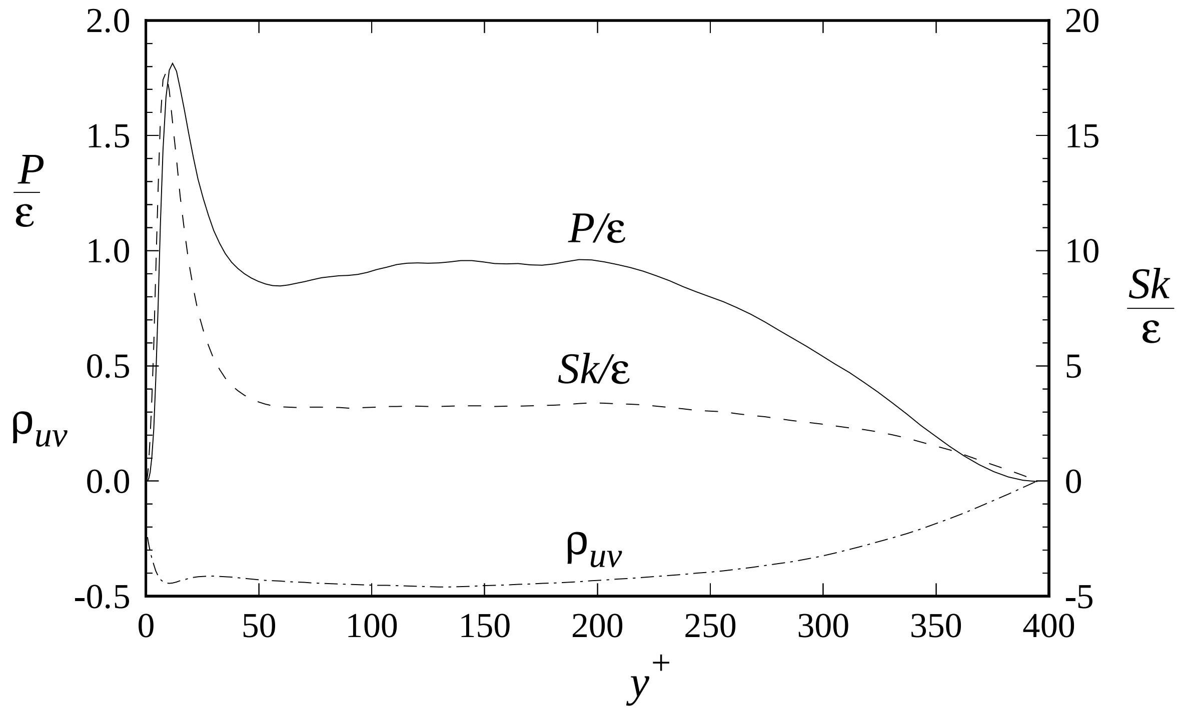

Figure 7.16: Profiles of the ratio of production to dissipation ($\mathcal{P}/\varepsilon$), normalized mean shear rate ($\mathcal{S}k/\varepsilon$), and shear stress correlation coefficient (ρ_{uv}) from DNS of channel flow at Re $= 13,750$ (Kim *et al.* 1987).

Turbulent Flows

Stephen B. Pope
Cambridge University Press, 2000

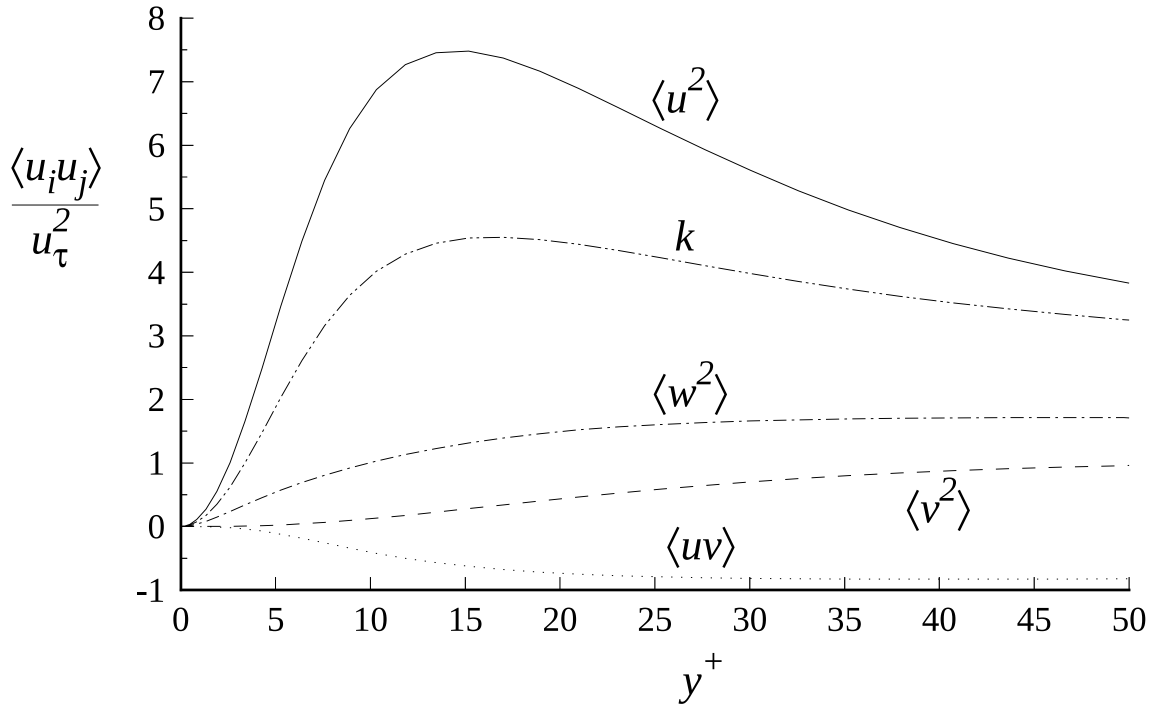

Figure 7.17: Profiles of Reynolds stresses and kinetic energy normalized by friction velocity in the viscous wall region of turbulent channel flow: DNS data of Kim *et al.* (1987) Re $= 13,750$.

Turbulent Flows

Stephen B. Pope
Cambridge University Press, 2000

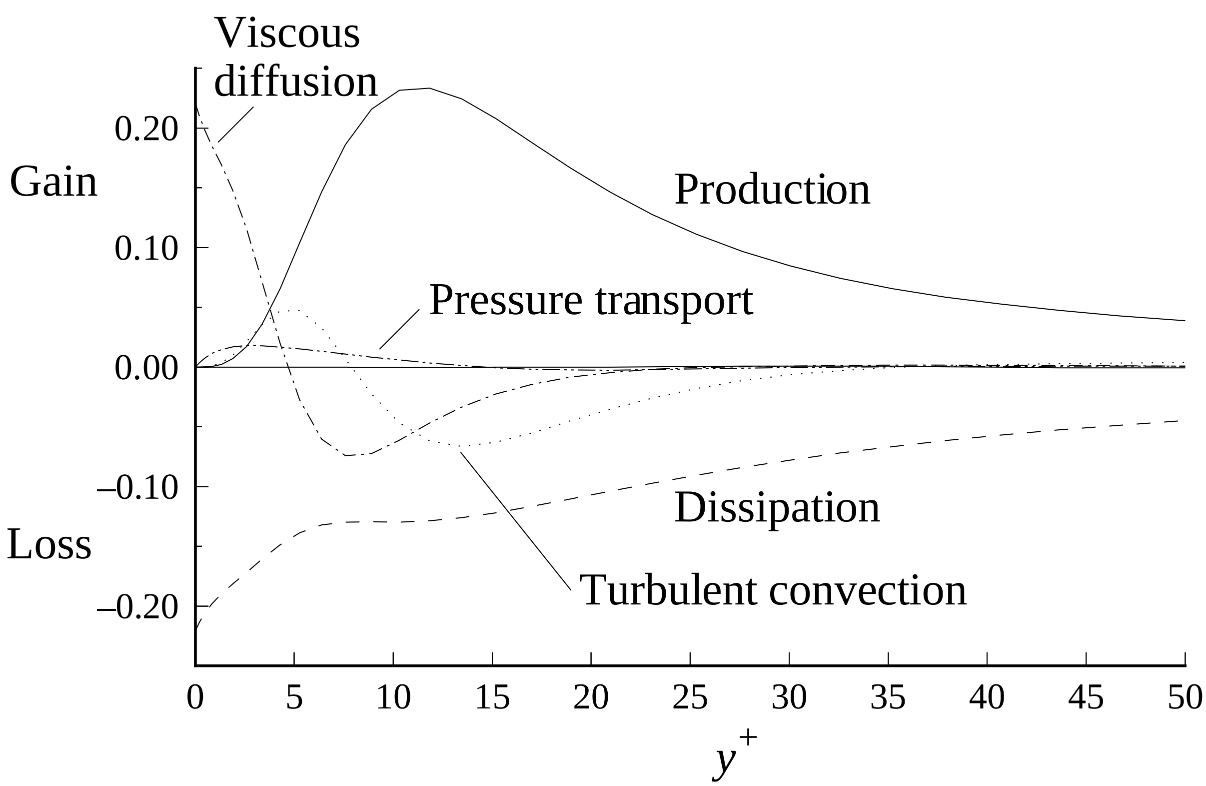

Figure 7.18: Turbulent kinetic energy budget in the viscous wall region of channel flow: terms in Eq. (7.64) normalized by viscous scales. From the DNS data of Kim *et al.* (1987) Re $= 13,750$.

Turbulent Flows

Stephen B. Pope
Cambridge University Press, 2000

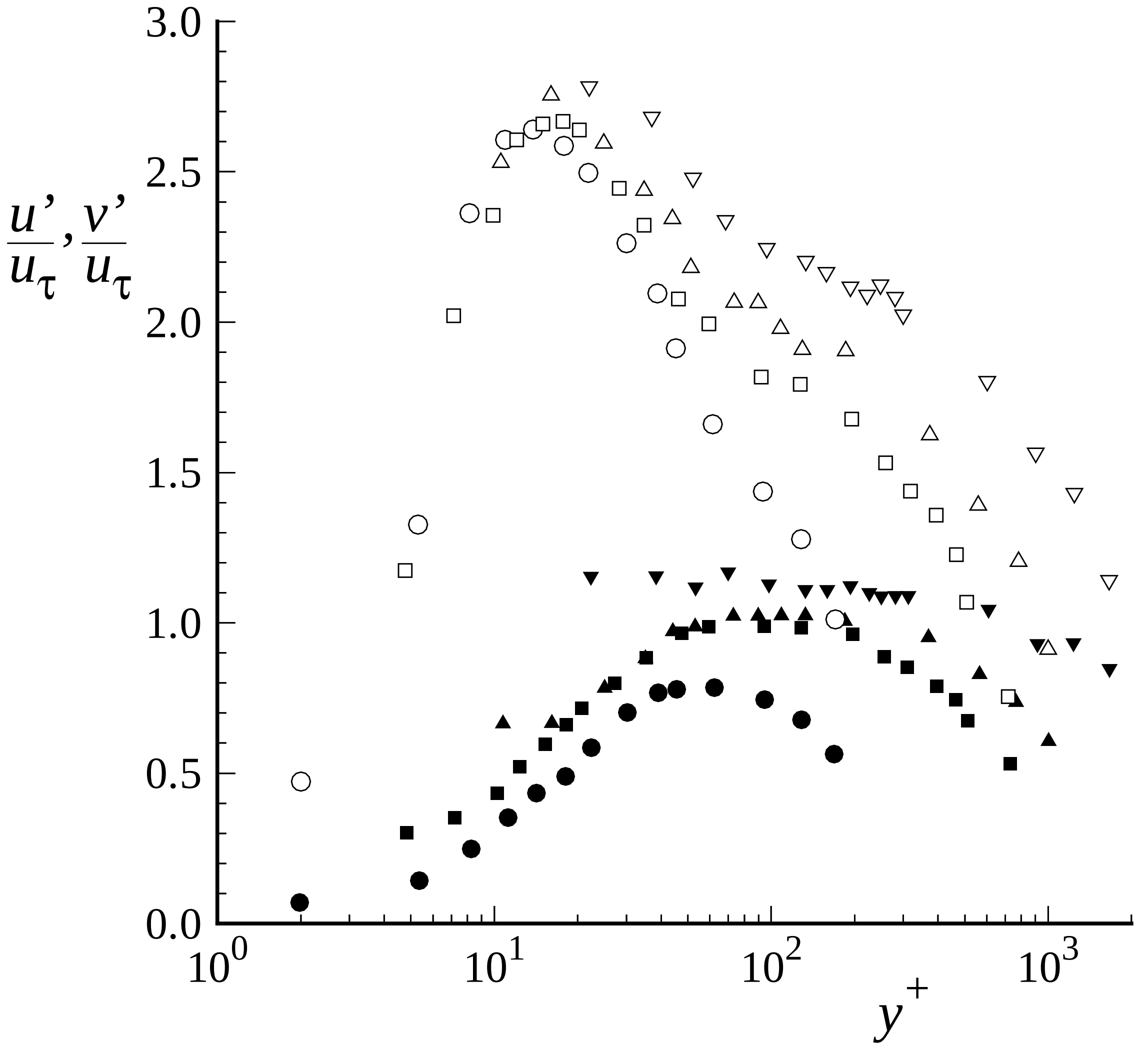

Figure 7.19: Profiles of r.m.s. velocity measured in channel flow at different Reynolds numbers by Wei and Willmarth (1989). Open symbols: $u'/u_\tau = \langle u^2 \rangle^{\frac{1}{2}}/u_\tau$; $\bigcirc, \mathrm{Re}_0 = 2,970$; $\square, \mathrm{Re}_0 = 14,914$; $\triangle, \mathrm{Re}_0 = 22,776$; $\bigtriangledown, \mathrm{Re}_0 = 39,582$. Solid symbols: $v'/u_\tau = \langle v^2 \rangle^{\frac{1}{2}}/u_\tau$ at the same Reynolds numbers.

Turbulent Flows

Stephen B. Pope
Cambridge University Press, 2000

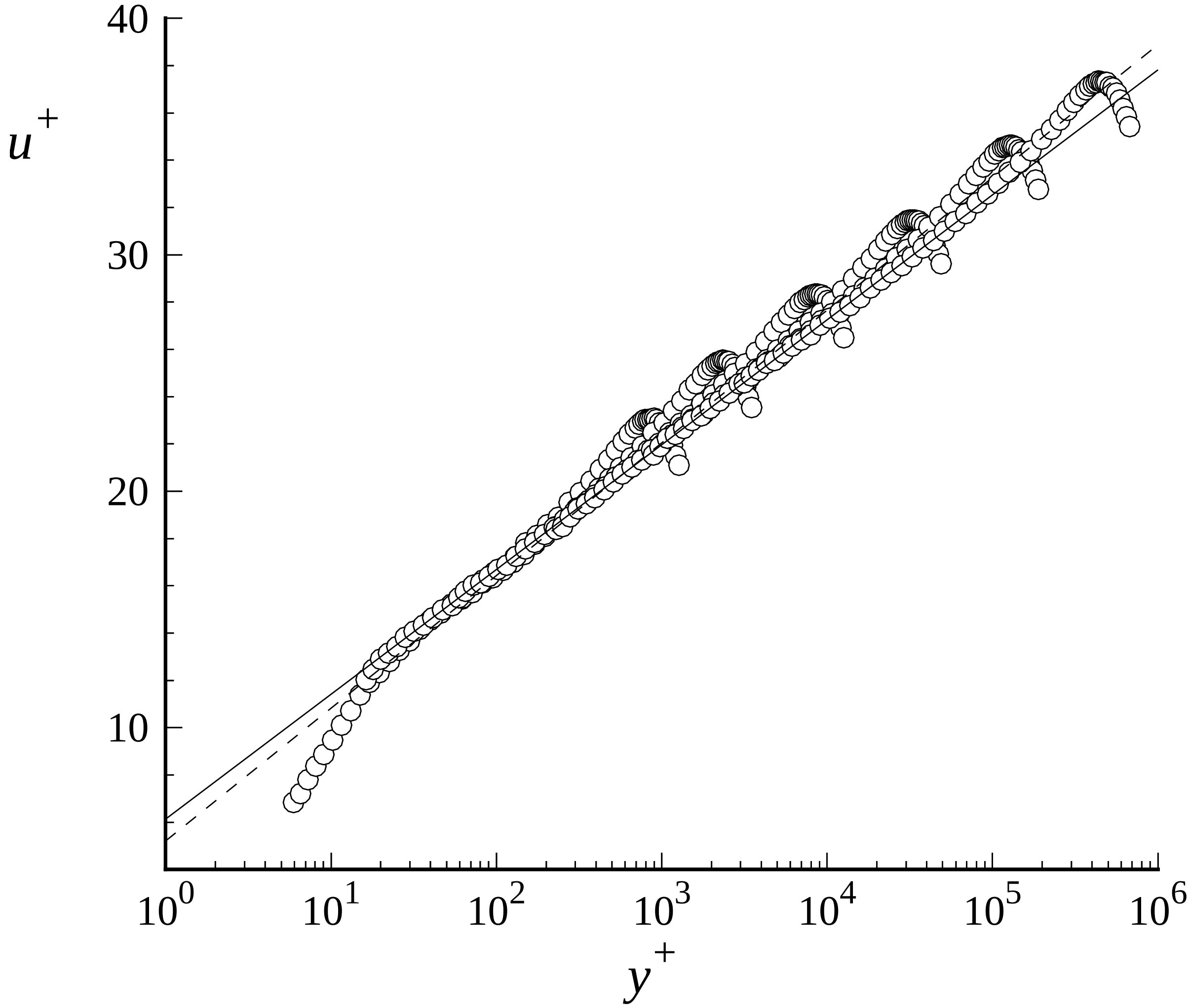

Figure 7.20: Mean velocity profiles in fully-developed turbulent pipe flow. Symbols, experimental data of Zagarola and Smits (1997) at six Reynolds numbers (Re $\approx 32\times10^3$, 99×10^3, 409×10^3, 1.79×10^6, 7.71×10^6, 29.9×10^6). Solid line, log law with $\kappa = 0.436$ and $B = 6.13$; dashed line, log law with $\kappa = 0.41$, $B = 5.2$.

Turbulent Flows

Stephen B. Pope
Cambridge University Press, 2000

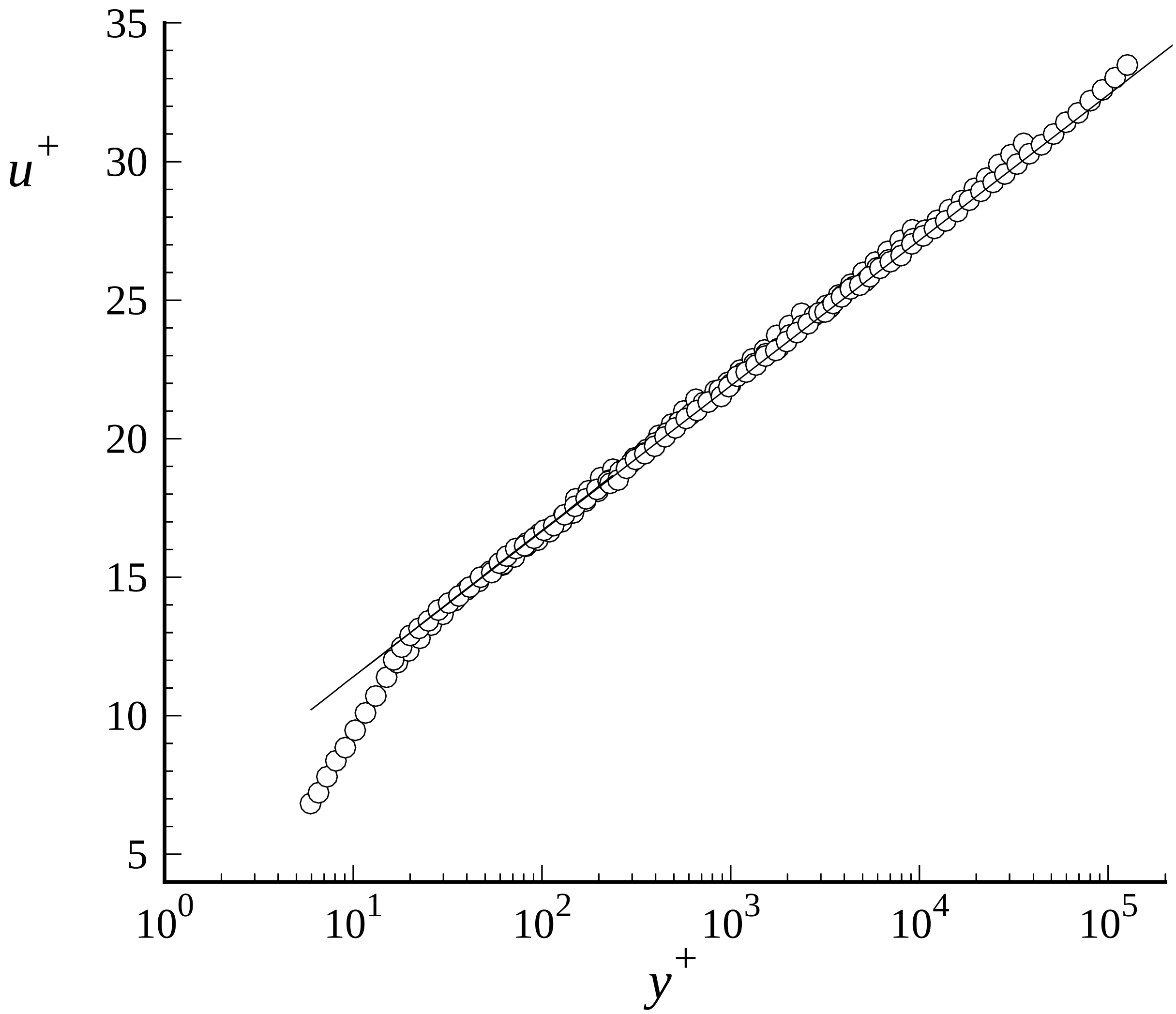

Figure 7.21: Mean velocity profiles in fully-developed turbulent pipe flow. Symbols, experimental data of Zagarola and Smits (1997) for $y/R < 0.1$, for the same values of Re as in Fig. 7.20. Line, log law with $\kappa = 0.436$ and $B = 6.13$.

Turbulent Flows

Stephen B. Pope
Cambridge University Press, 2000

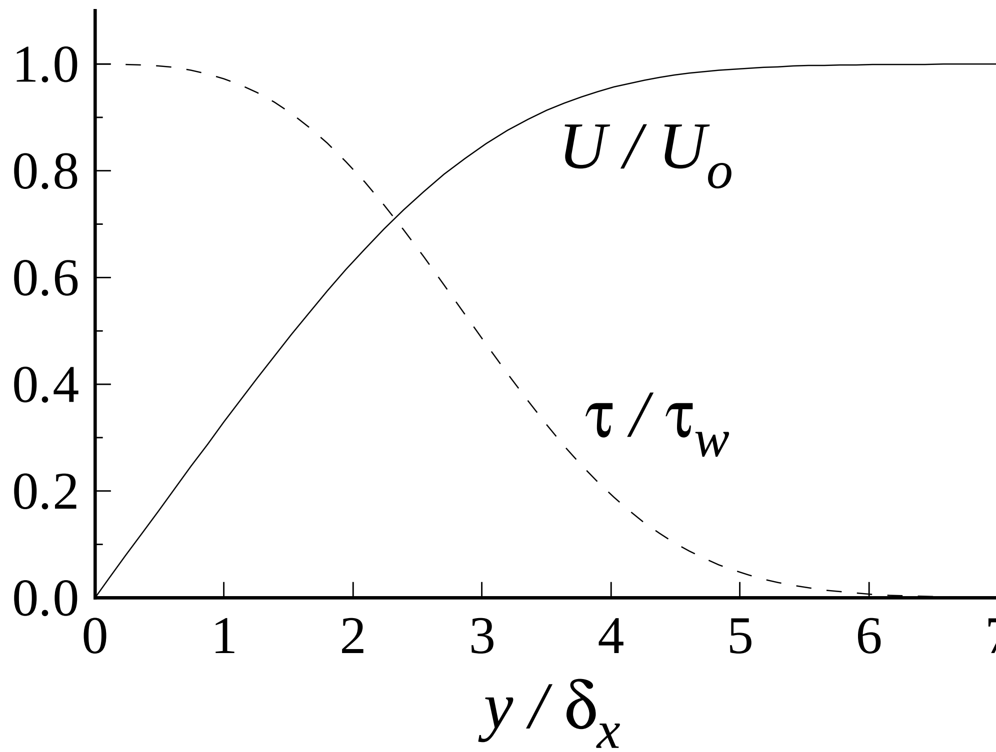

Figure 7.25: Normalized velocity and shear stress profiles from the Blasius solution for the zero-pressure-gradient laminar boundary layer on a flat plate: y is normalized by $\delta_x \equiv x/\mathrm{Re}_x^{\frac{1}{2}} = (x\nu/U_0)^{\frac{1}{2}}$.

Turbulent Flows

Stephen B. Pope
Cambridge University Press, 2000

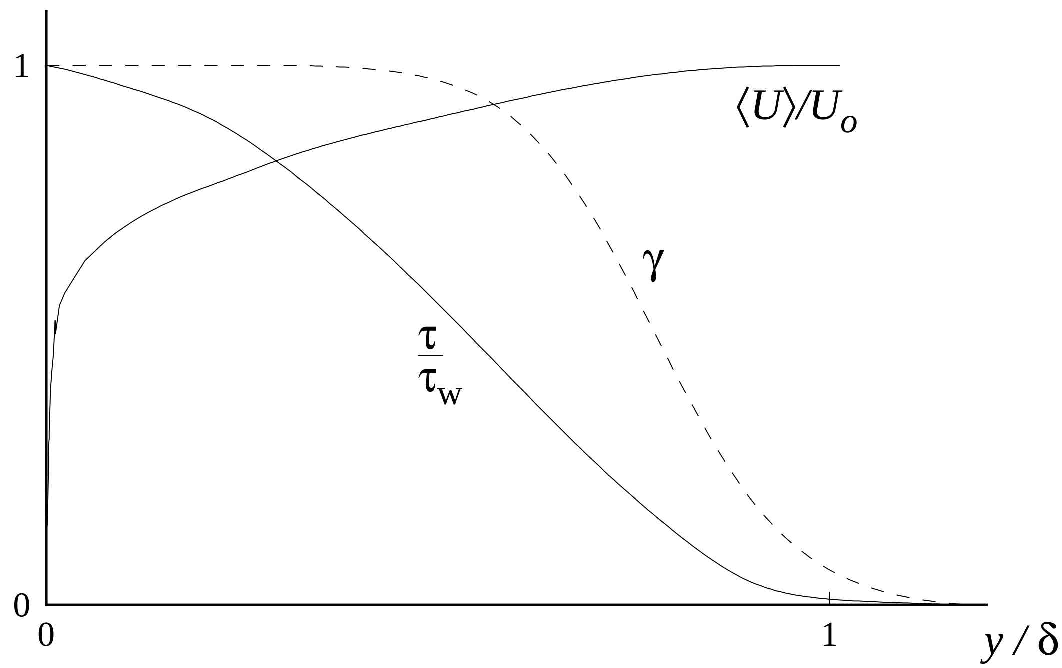

Figure 7.26: Profiles of mean velocity, shear stress and intermittency factor in a zero-pressure gradient turbulent boundary layer, $\mathrm{Re}_\theta = 8,000$. From the experimental data of Klebanoff (1954).

Turbulent Flows

Stephen B. Pope
Cambridge University Press, 2000

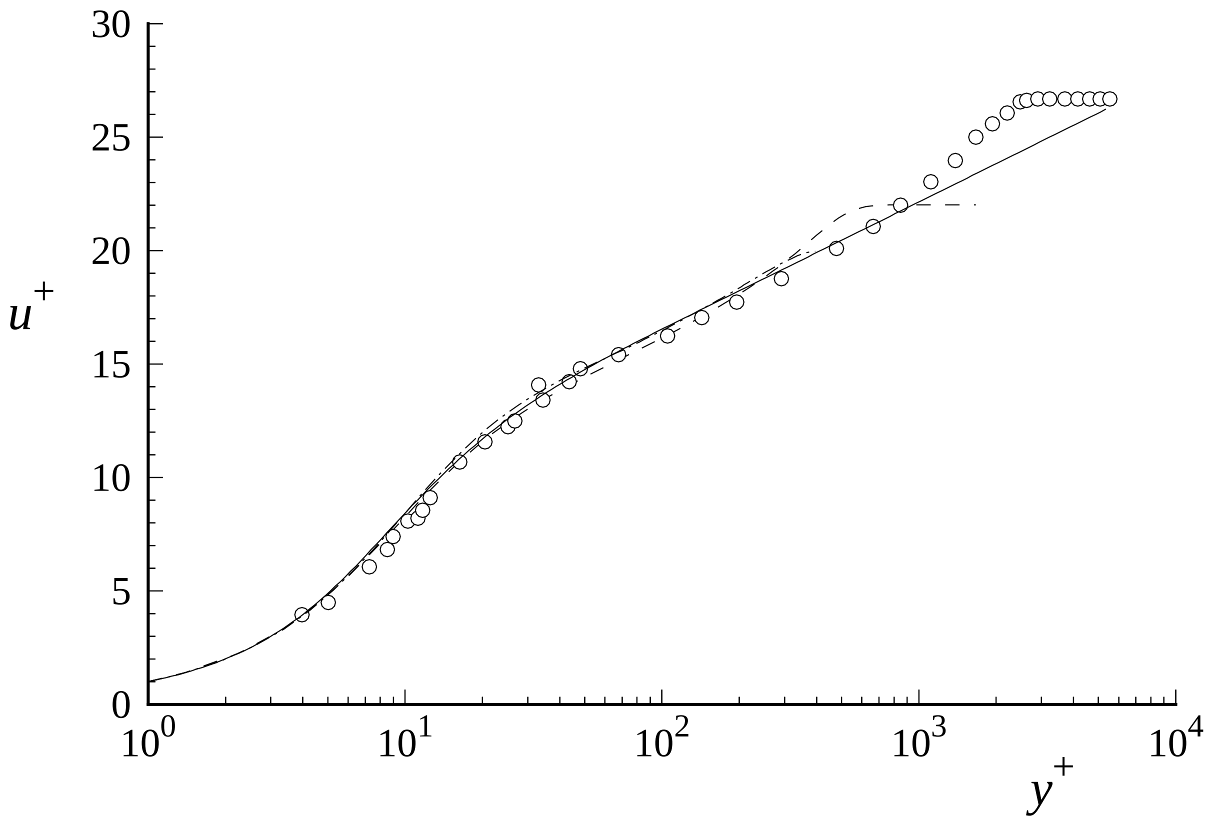

Figure 7.27: Mean velocity profiles in wall units. Circles, boundary-layer experiments of Klebanoff (1954), $\mathrm{Re}_\theta = 8,000$; dashed line, boundary-layer DNS of Spalart (1988), $\mathrm{Re}_\theta = 1,410$; dot-dashed line, channel flow DNS of Kim *et al.* (1987), $\mathrm{Re} = 13,750$; solid line, van Driest's law of the wall, Eqs. (7.144)–(7.145).

Turbulent Flows

Stephen B. Pope
Cambridge University Press, 2000

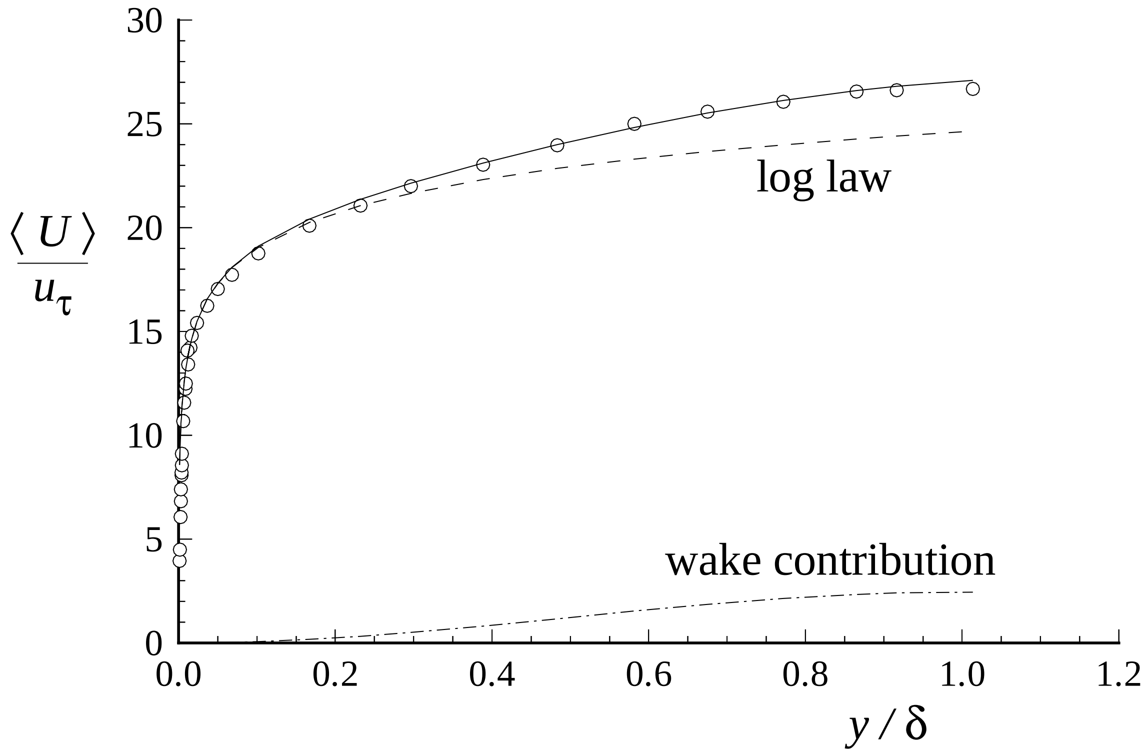

Figure 7.28: Mean velocity profile in a turbulent boundary layer showing the law of the wake. Symbols, experimental data of Klebanoff (1954); dashed line, log law ($\kappa = 0.41, B = 5.2$); dot-dashed line, wake contribution $\Pi w(y/\delta)/\kappa$ ($\Pi = 0.5$); solid line, sum of log law and wake contribution (Eq. 7.148).

Turbulent Flows

Stephen B. Pope
Cambridge University Press, 2000

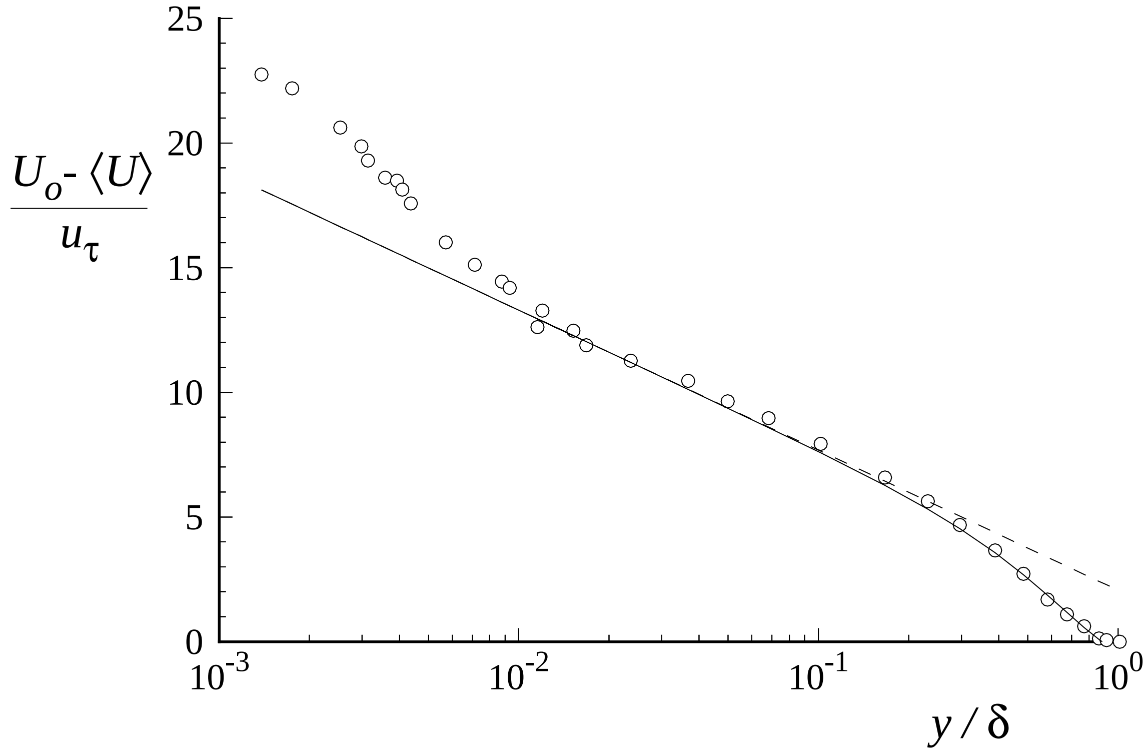

Figure 7.29: Velocity defect law. Symbols, experimental data of Klebanoff (1954); dashed line, log law; solid line, sum of log law and wake contribution $\Pi w(y/\delta)/\kappa$.

Turbulent Flows

Stephen B. Pope
Cambridge University Press, 2000

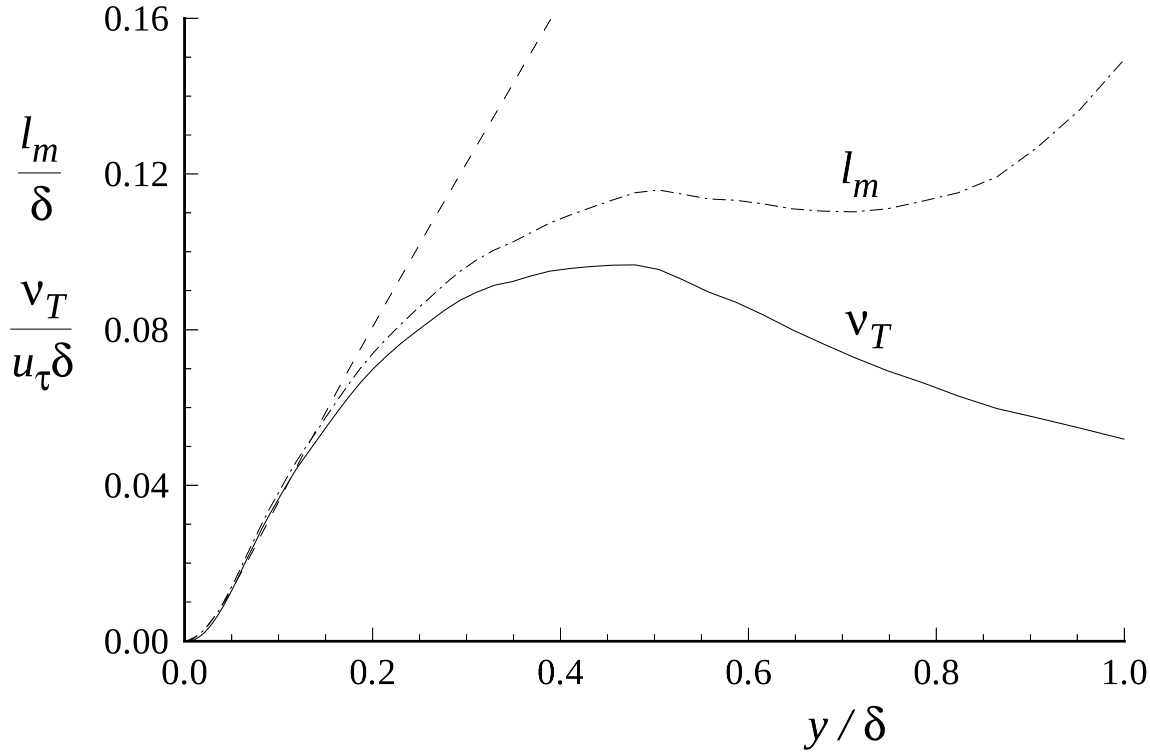

Figure 7.30: Turbulent viscosity and mixing length deduced from direct numerical simulations of a turbulent boundary layer (Spalart 1988). Solid line, ν_T from DNS; dot-dash line, ℓ_m from DNS; dashed line ℓ_m and ν_T according to van Driest's specification (Eq. 7.145).

Turbulent Flows

Stephen B. Pope

Cambridge University Press, 2000

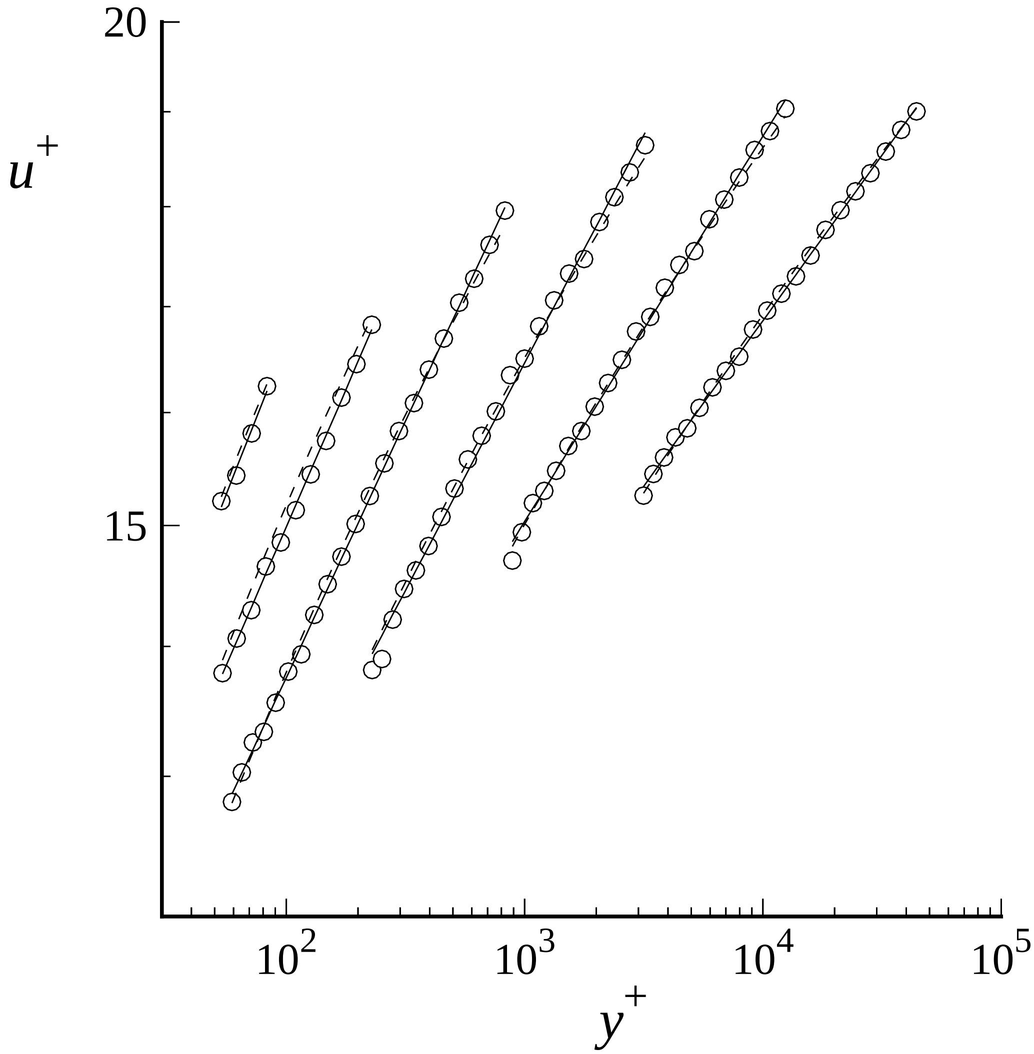

Figure 7.31: Log-log plot of mean velocity profiles in turbulent pipe flow at six Reynolds number (from left to right: Re $\approx 32 \times 10^3$, 99×10^3, 409×10^3, 1.79×10^6, 7.71×10^6, 29.9×10^6). The scale for u^+ pertains to the lowest Reynolds number: subsequent profiles are shifted down successively by a factor of 1.1. The range shown is the overlap region, $50\delta_\nu < y < 0.1\,R$. Symbols, experimental data of Zagarola and Smits (1997); dashed lines, log law with $\kappa = 0.436$ and $B = 6.13$; solid lines, power law (Eq. 7.157) with the power α determined by the best fit to the data.

Turbulent Flows

Stephen B. Pope
Cambridge University Press, 2000

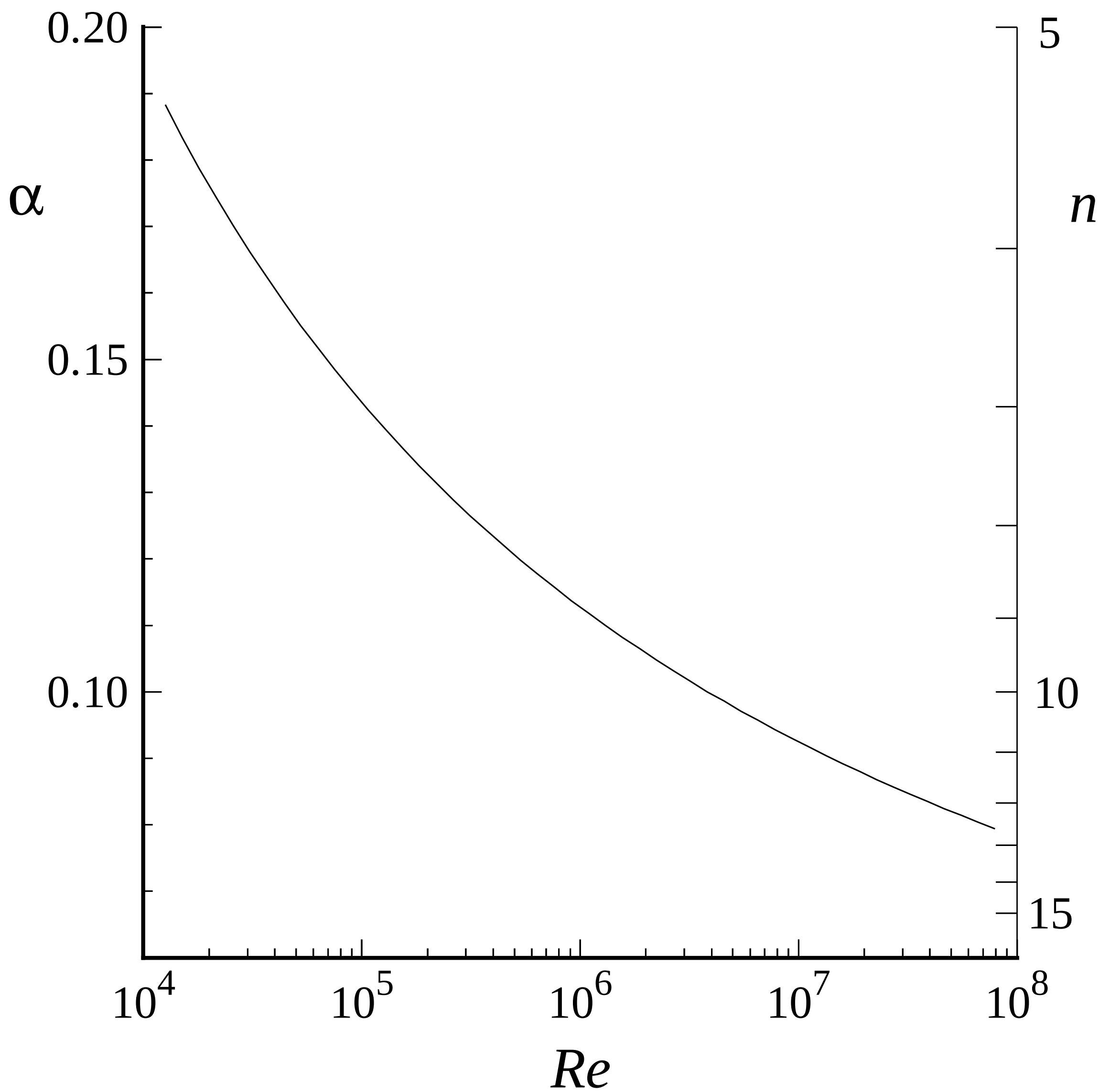

Figure 7.32: Exponent $\alpha = 1/n$ (Eq. 7.158) in the power-law $u^+ = C(y^+)^\alpha = C(y^+)^{1/n}$ for pipe flow as a function of Reynolds number.

Turbulent Flows

Stephen B. Pope
Cambridge University Press, 2000

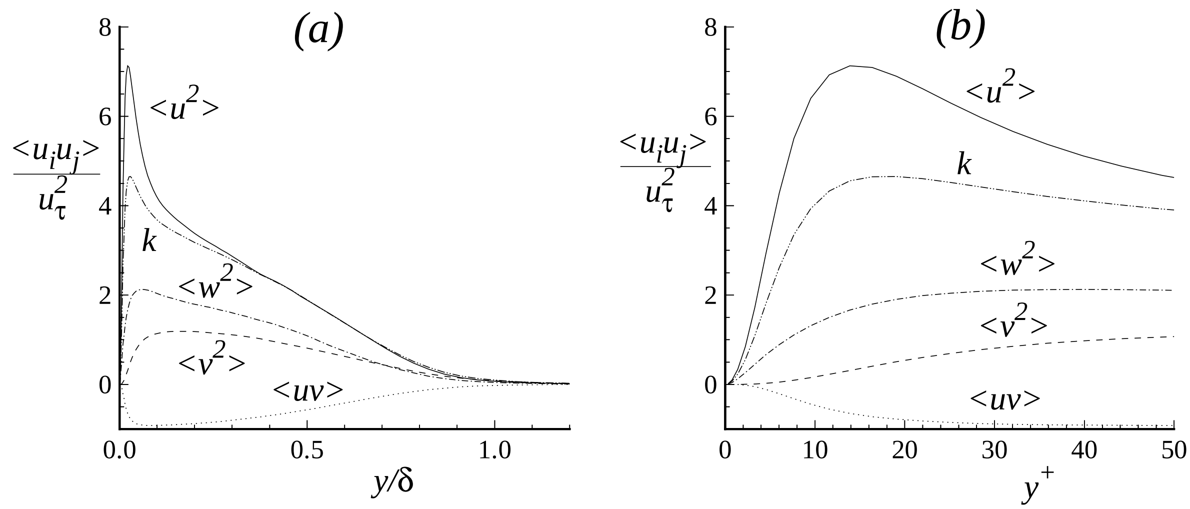

Figure 7.33: Profiles of Reynolds stresses and kinetic energy normalized by the friction velocity in a turbulent boundary layer at $\mathrm{Re}_\theta = 1,410$: (a) across the boundary layer (b) in the viscous near-wall region. From the DNS data of Spalart (1988).

Turbulent Flows

Stephen B. Pope
Cambridge University Press, 2000

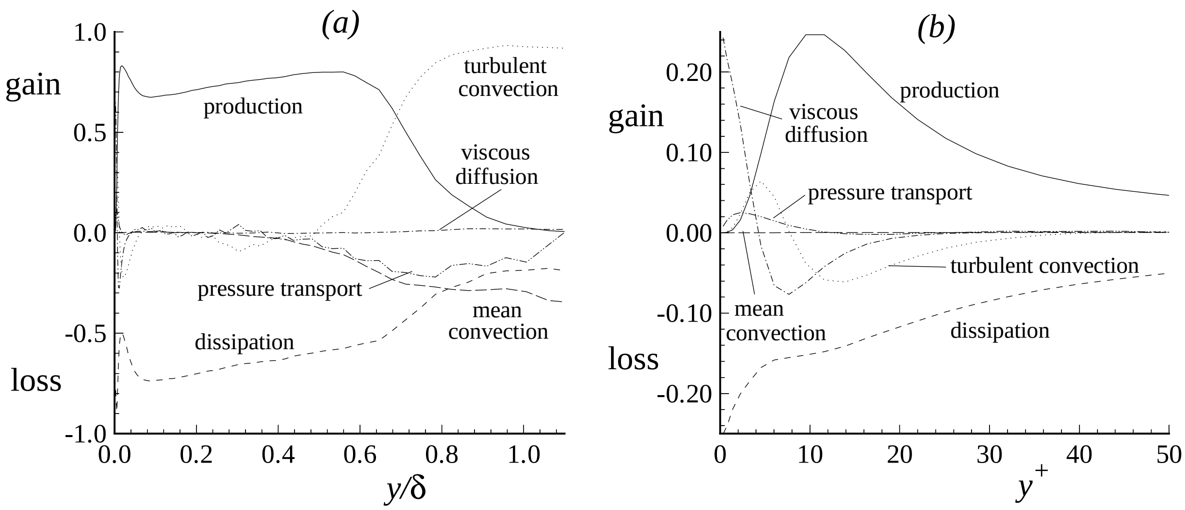

Figure 7.34: Turbulent kinetic energy budget in a turbulent boundary layer at $\mathrm{Re}_\theta = 1,410$: terms in Eq. (7.177) (a) normalized as a function of y so that the sum of the squares of the terms is unity (b) normalized by the viscous scales. From the DNS data of Spalart (1988).

Turbulent Flows

Stephen B. Pope
Cambridge University Press, 2000

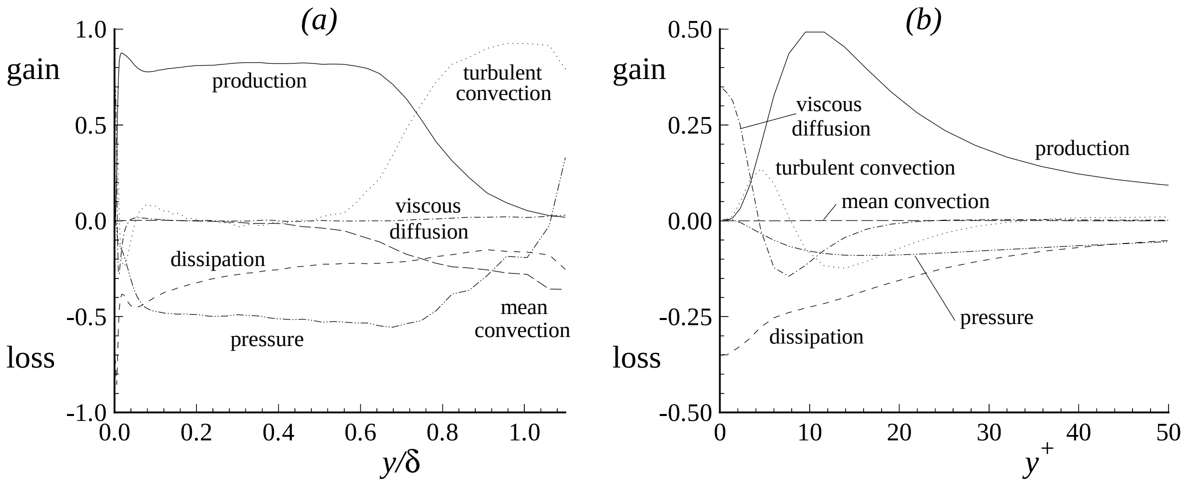

Figure 7.35: Budget of $\langle u^2 \rangle$ in a turbulent boundary layer: conditions and normalization are the same as in Fig. 7.34.

Turbulent Flows

Stephen B. Pope
Cambridge University Press, 2000

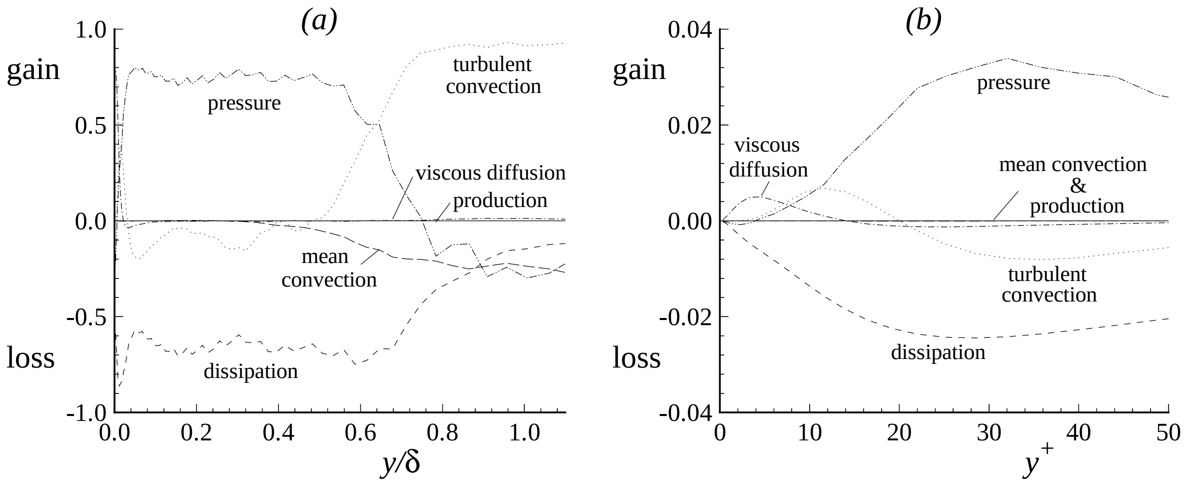

Figure 7.36: Budget of $\langle v^2 \rangle$ in a turbulent boundary layer: conditions and normalization are the same as in Fig. 7.34.

Turbulent Flows

Stephen B. Pope
Cambridge University Press, 2000

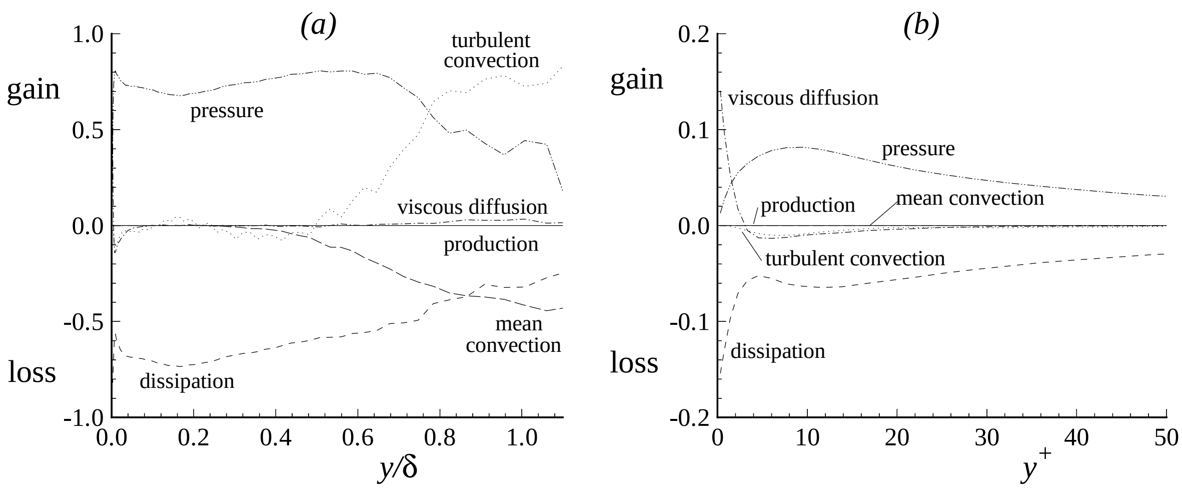

Figure 7.37: Budget of $\langle w^2 \rangle$ in a turbulent boundary layer: conditions and normalization are the same as in Fig. 7.34.

Turbulent Flows

Stephen B. Pope

Cambridge University Press, 2000

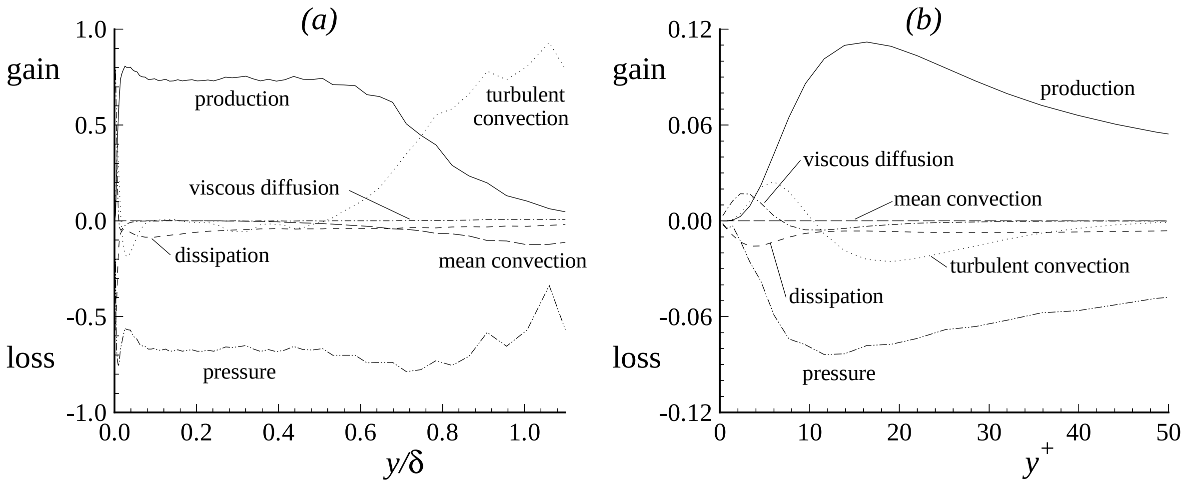

Figure 7.38: Budget of $-\langle uv\rangle$ in a turbulent boundary layer: conditions and normalization are the same as in Fig. 7.34.

Turbulent Flows

Stephen B. Pope
Cambridge University Press, 2000

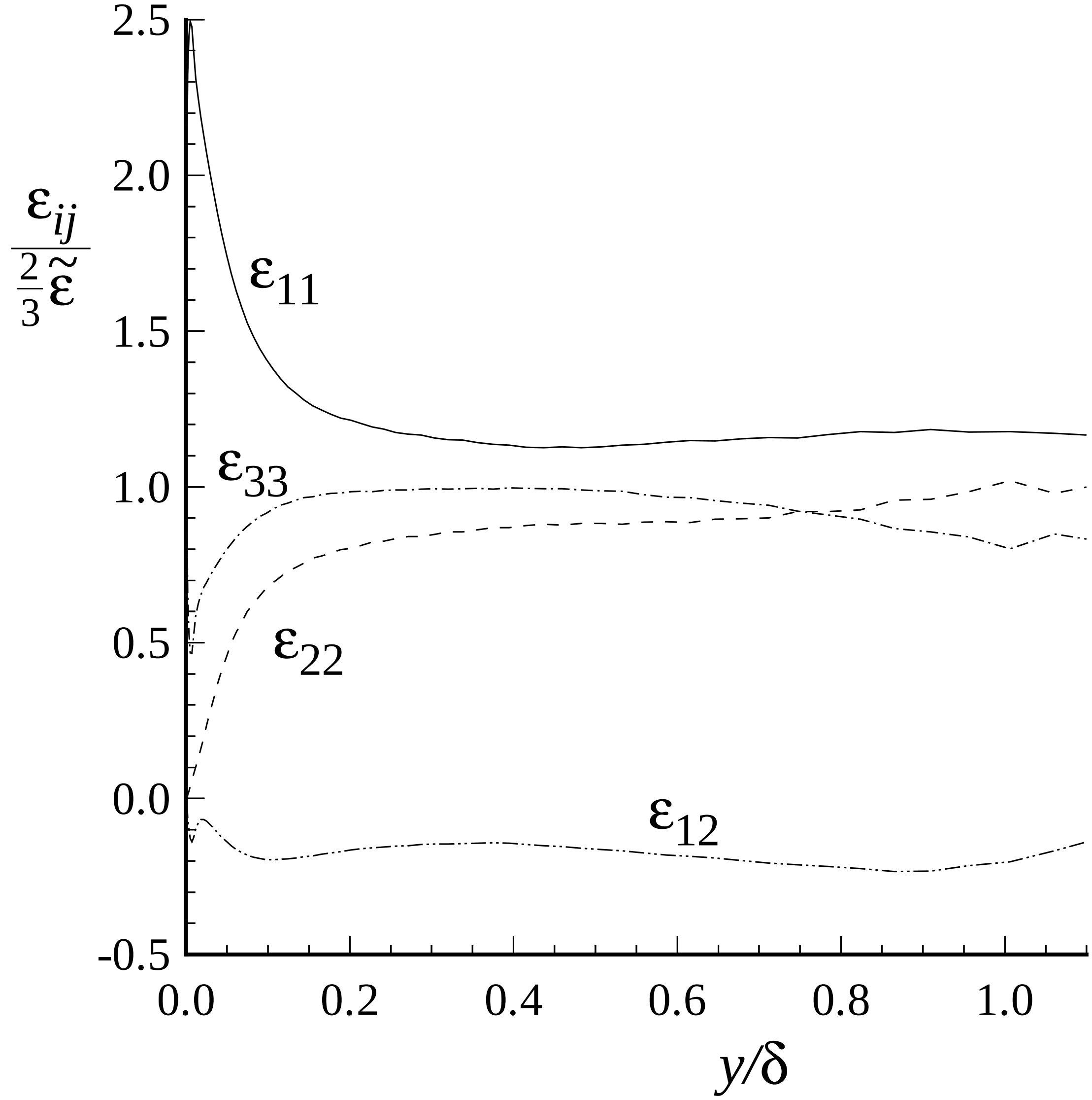

Figure 7.39: Normalized dissipation components in a turbulent boundary layer at $\mathrm{Re}_\theta = 1,410$: from the DNS data of Spalart (1988) for which $\delta = 650\delta_\nu$.

Turbulent Flows

Stephen B. Pope
Cambridge University Press, 2000

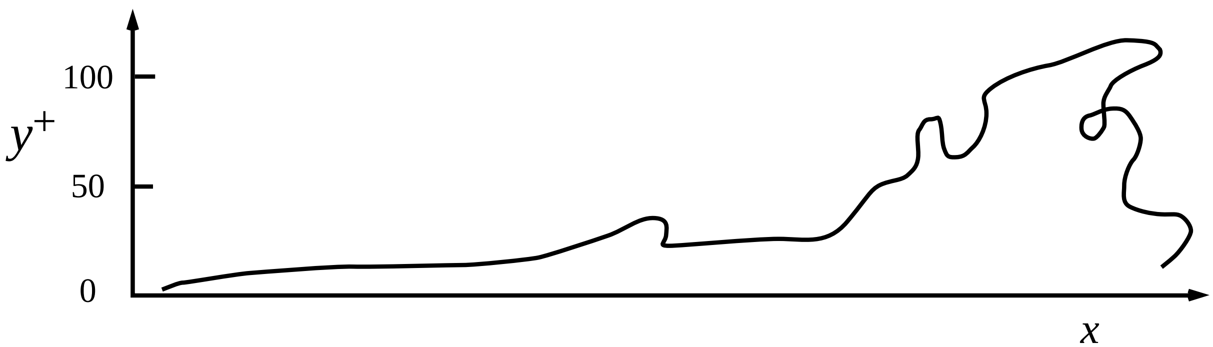

Figure 7.40: Dye streak in a turbulent boundary layer showing the ejection of low-speed near-wall fluid. (From the experiment of Kline *et al.* 1967.)

Turbulent Flows

Stephen B. Pope

Cambridge University Press, 2000

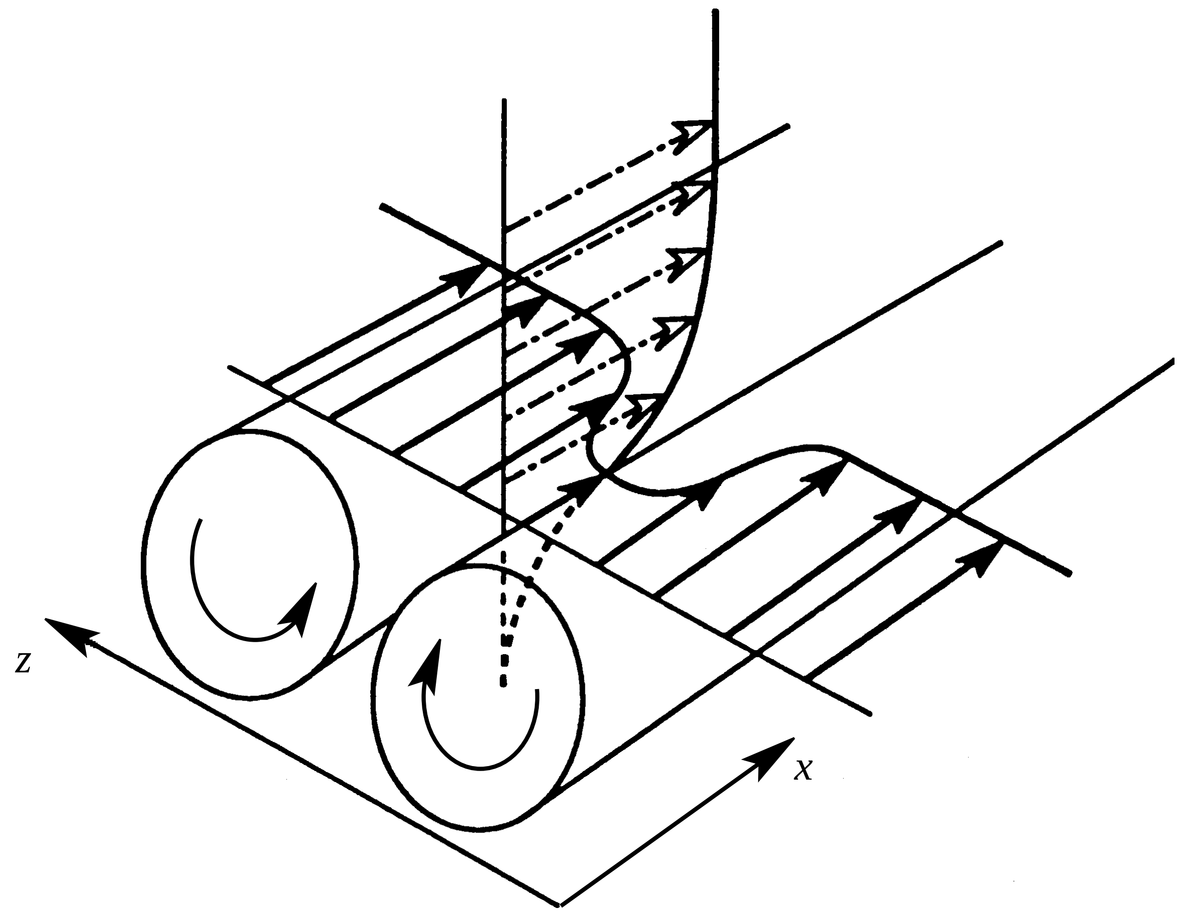

Figure 7.42: Sketch of counter-rotating rolls in the near-wall region. (From Holmes *et al.* 1996.)

Turbulent Flows

Stephen B. Pope

Cambridge University Press, 2000

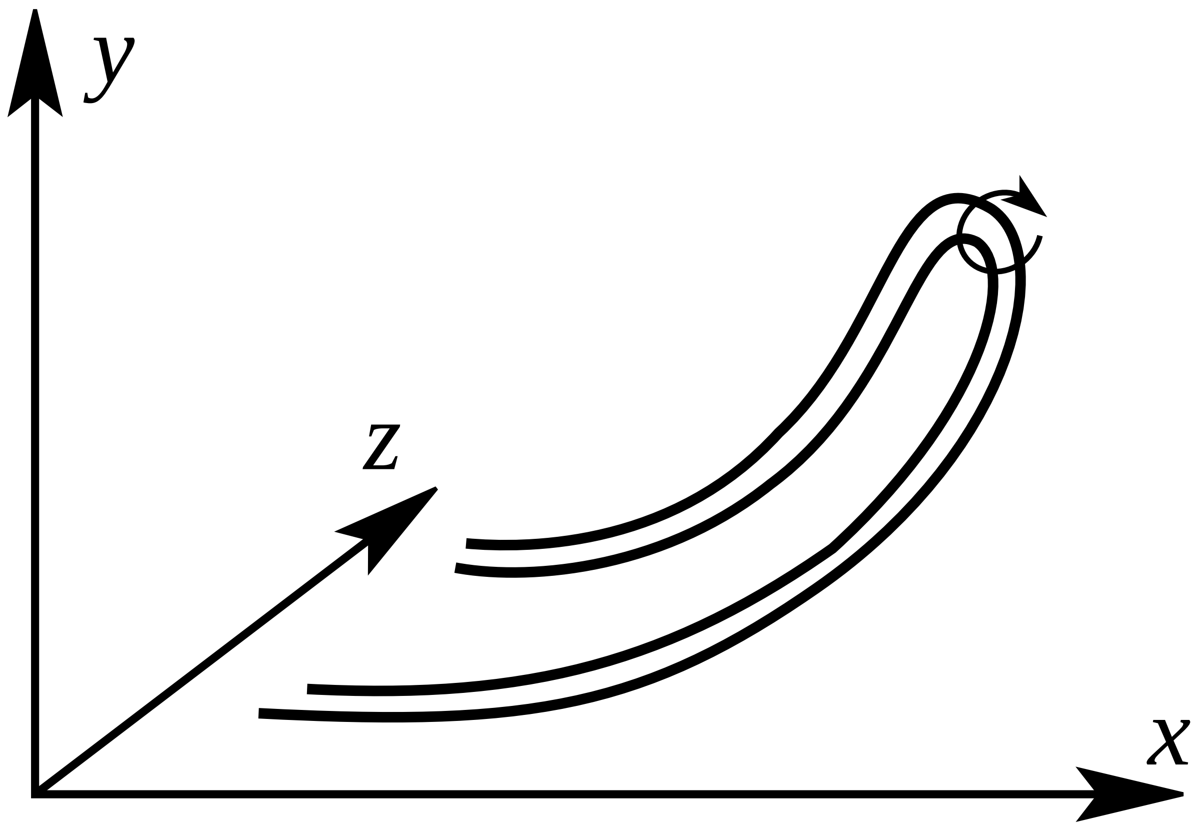

Figure 7.43: Sketch of counter-rotating rolls in the near-wall region. (From Holmes *et al.* 1996.)

Turbulent Flows

Stephen B. Pope
Cambridge University Press, 2000

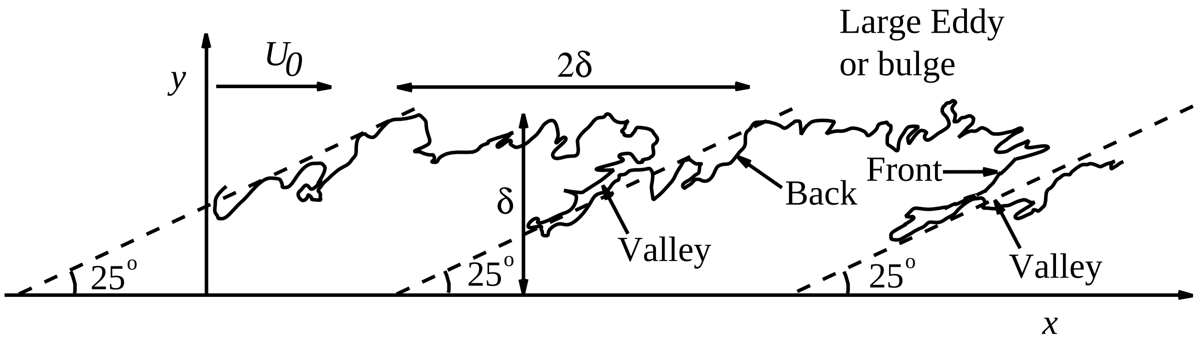

Figure 7.44: The large-scale features of a turbulent boundary layer at $\mathrm{Re}_\theta \approx 4,000$. The irregular line—approximating the viscous superlayer—is the boundary between smoke-filled turbulent fluid and clear free-stream fluid. (From the experiment of Falco 1977.)